Supplementary Materials for Trigonal prismatic coordination geometry imparted by a macrocyclic ligand: an approach to large axial magnetic anisotropy for Co(II)

Eva Zahradníková,[a] Jean-Pascal Sutter,[b*] Petr Halaš[a] and Bohuslav Drahoš[a*]

[a] *Department of Inorganic Chemistry, Faculty of Science, Palacký University Olomouc, 17. listopadu 12, CZ-771 46 Olomouc, Czech Republic, Fax: +420 585 634 954. Tel: +420 585 634 429. E-mail: bohuslav.drahos@upol.cz*
[b] *Laboratoire de Chimie de Coordination du CNRS (LCC-CNRS), Université de Toulouse, CNRS, Toulouse, France. E-mail: jean-pascal.sutter@lcc-toulouse.fr*

Table of content:

Figure S17 Results of CASSCF/NEVPT2 calculations for the complex **1b** showing the molecular fragment $[Co(L)X]^+$ overlaid with the principal axes of the *D*-tensor, AILFT d-orbital splitting together with their visualisation and composition.

Figure S18 Results of CASSCF/NEVPT2 calculations for the complex **2** (first crystallographically independent molecule in the asymmetric unit) showing the molecular fragment $[Co(L)X]^+$ overlaid with the principal axes of the *D*-tensor, AILFT d-orbital splitting together with their visualisation and composition.

Figure S19 Results of CASSCF/NEVPT2 calculations for the complex **2** (second crystallographically independent molecule in the asymmetric unit) showing the molecular fragment $[Co(L)X]^+$ overlaid with the principal axes of the *D*-tensor, AILFT d-orbital splitting together with their visualisation and composition.

Figure S20 Results of CASSCF/NEVPT2 calculations for the complex **3** showing the molecular fragment $[Co(L)X]^+$ overlaid with the principal axes of the *D*-tensor, AILFT d-orbital splitting together with their visualisation and composition.

Figure S21 Results of CASSCF/NEVPT2 calculations for the complex **4** showing the molecular fragment $[Co(L)X]^+$ overlaid with the principal axes of the *D*-tensor, AILFT d-orbital splitting together with their visualisation and composition.

Figure S22 Results of CASSCF/NEVPT2 calculations for the complex **5** showing the molecular fragment $[Co(L)X]^+$ overlaid with the principal axes of the *D*-tensor, AILFT d-orbital splitting together with their visualisation and composition.

Figure S23 Results of CASSCF/NEVPT2 calculations for the complex **6** showing the molecular fragment $[Co(L)X]^+$ overlaid with the principal axes of the *D*-tensor, AILFT d-orbital splitting together with their visualisation and composition.

Table S1 Results of continuous shape measures calculations using program Shape 2.1 for complexes **1–6**.

Table S2 Selected bond angles (°) for the studied complexes **1–6**.

Table S3 Calculated individual non-zero contributions to *D*-tensor for studied complexes **1**–**6** obtained from the CASSCF/NEVPT2 calculation together with the major contributing electronic configurations corresponding to the computed electronic states.

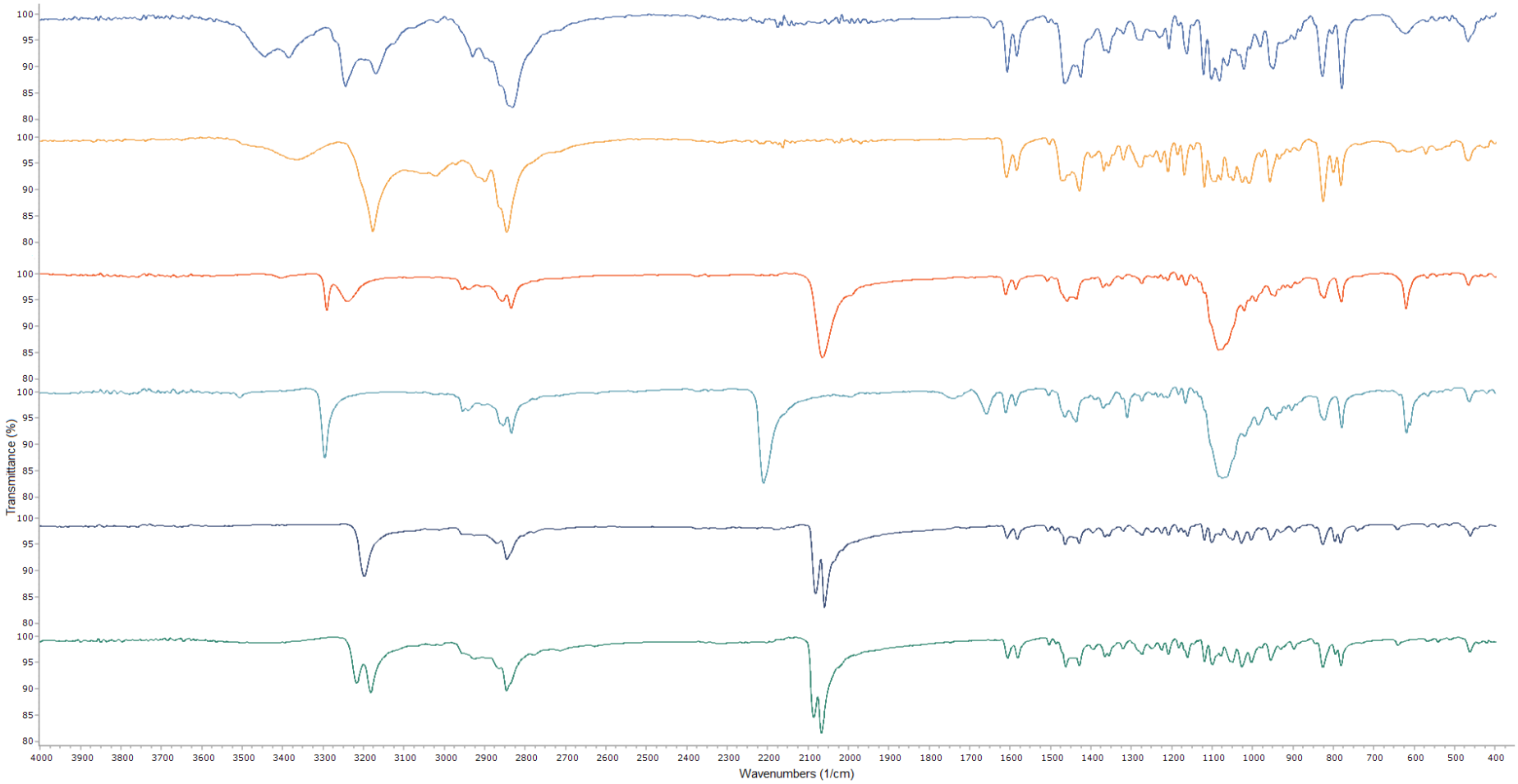

Figure S1 Comparison of IR spectra of studied complexes **1a**–**6**. Curve colors: blue = **1a**; yellow = **2**; red = **3**; turquoise = **4**; grey = **5**, green = **6**.

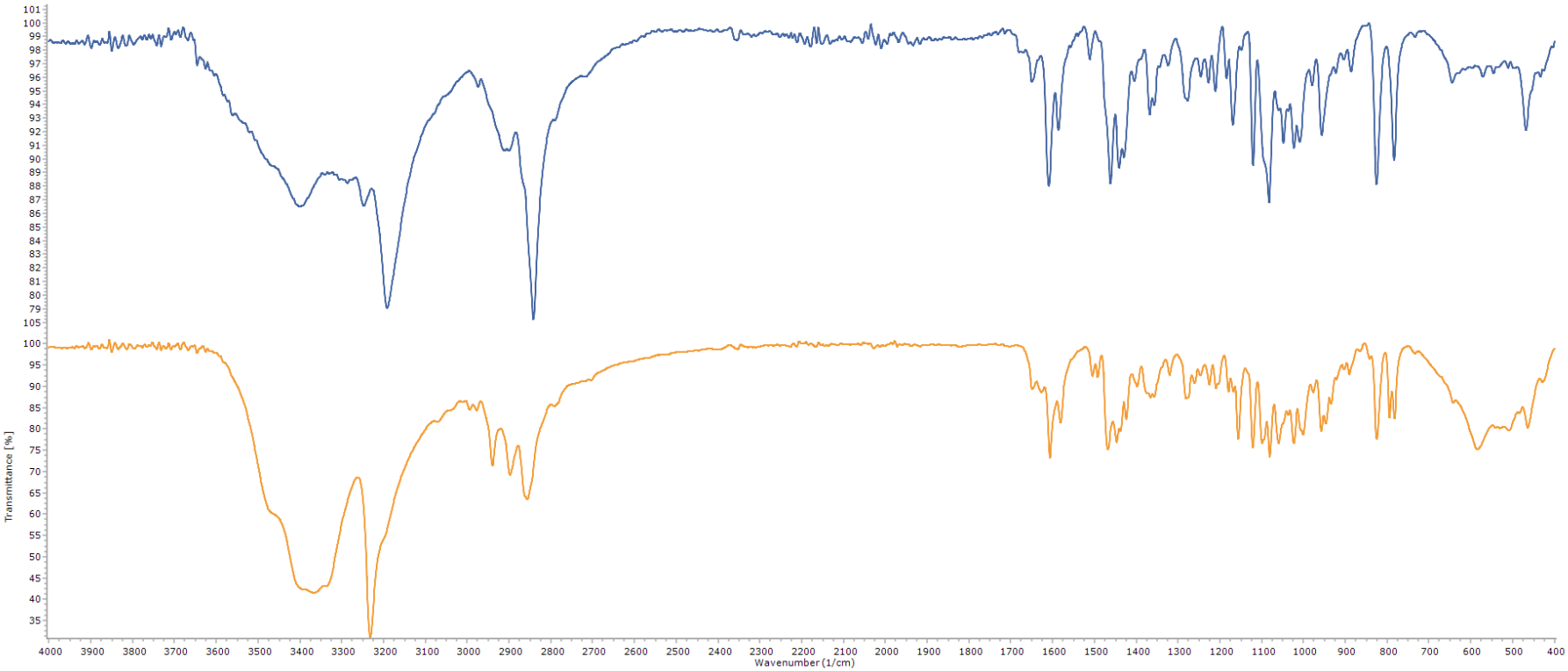

Figure S2 Comparison of IR spectra of studied complexes **1a** (*blue*) and **1b** (*yellow*).

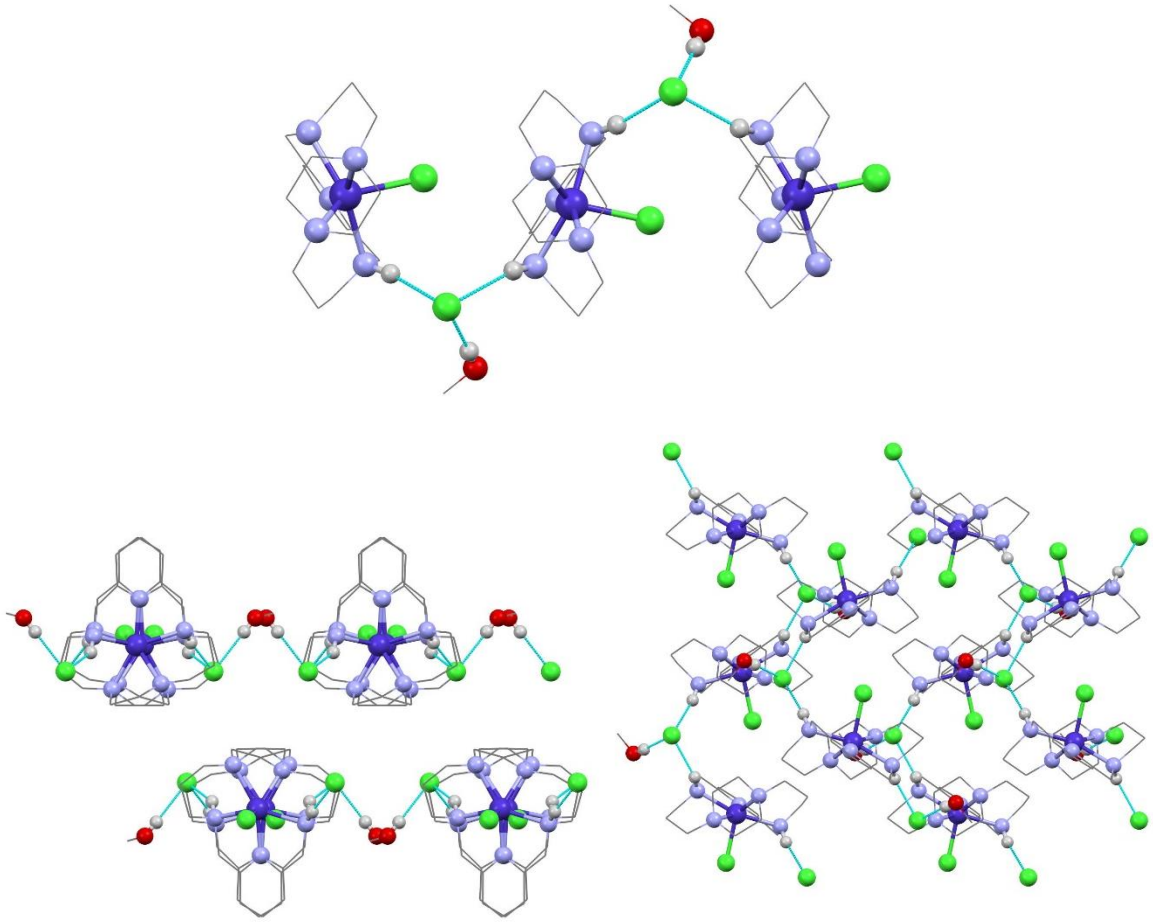

Figure S3 The crystal packing of complex [Co**L**Cl]Cl·CH_3OH·0.5CH_3NO_2 (**1a**). View of the supramolecular 1D chain (*top*), view along b axis (*bottom left*) and view along c axis (*bottom right*). Blue dashed lines represent hydrogen bonds.

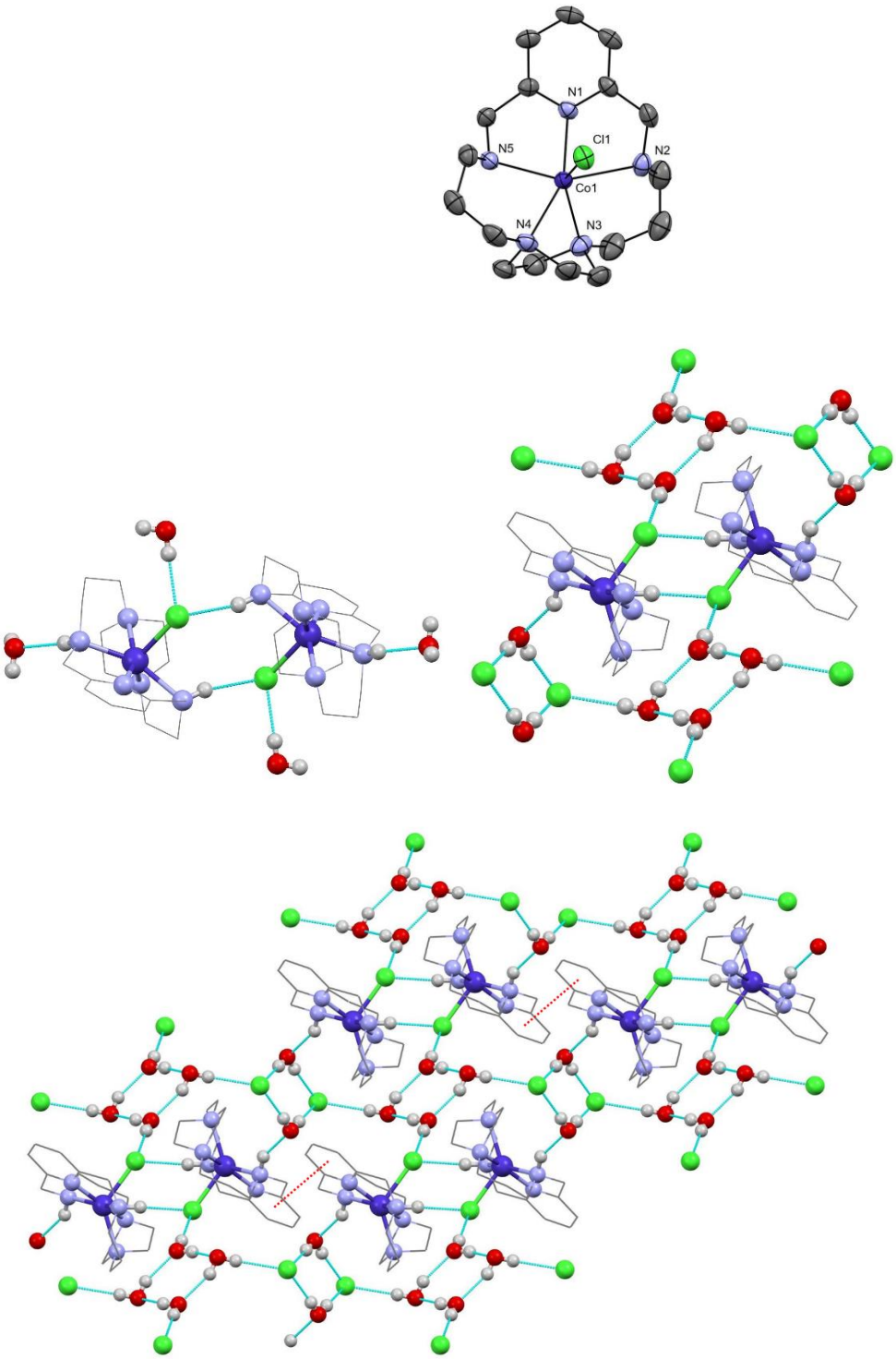

Figure S4 The molecular structures of the [Co**L**(X)]+ cations found in the crystal structure of complex [Co**L**Cl]Cl·3H_2O (**1b**) (*top*, non-hydrogen atoms are drawn as thermal ellipsoids at the 50% probability level, hydrogen atoms and anions were omitted for clarity). The view of crystal packing of complex **1b** showing hydrogen bonds in the supramolecular dimer (*middle left*), view along b axis on the extensive system of hydrogen bonds in the same dimer with more water molecules and chloride anoints (*middle right*), and view along b axis (*bottom*) on the connection of the supramolecular dimers into 1D chains and their connection between each other. Blue dashed lines represent hydrogen bonds and red dashed lines π-π stacking interactions.

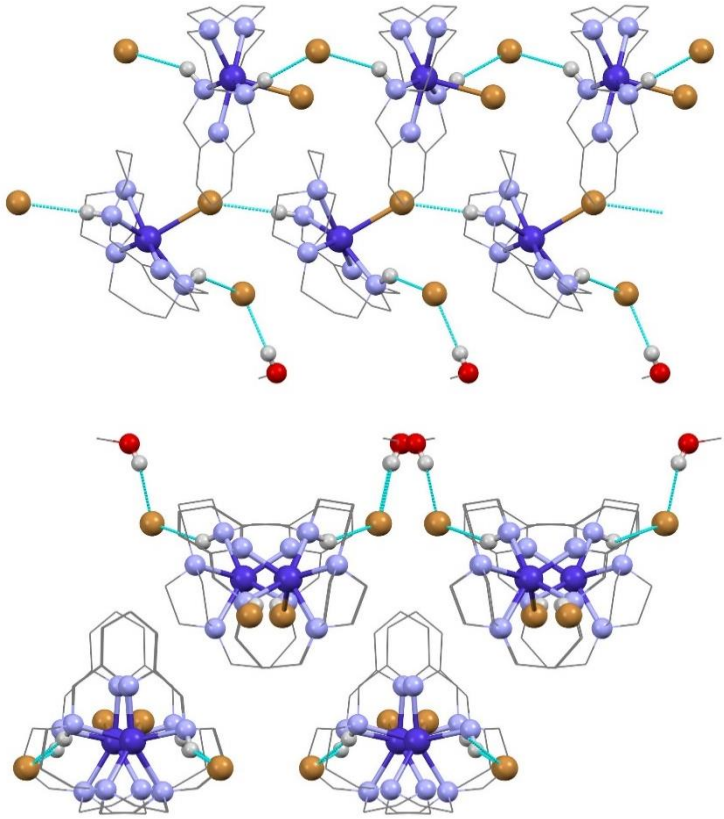

Figure S5 The crystal packing of complex [Co**L**Br]Br·0.5CH_3OH (**2**). View of the supramolecular 1D chains along b axis (*top*) and along c axis (*bottom*). Blue dashed lines represent hydrogen bonds.

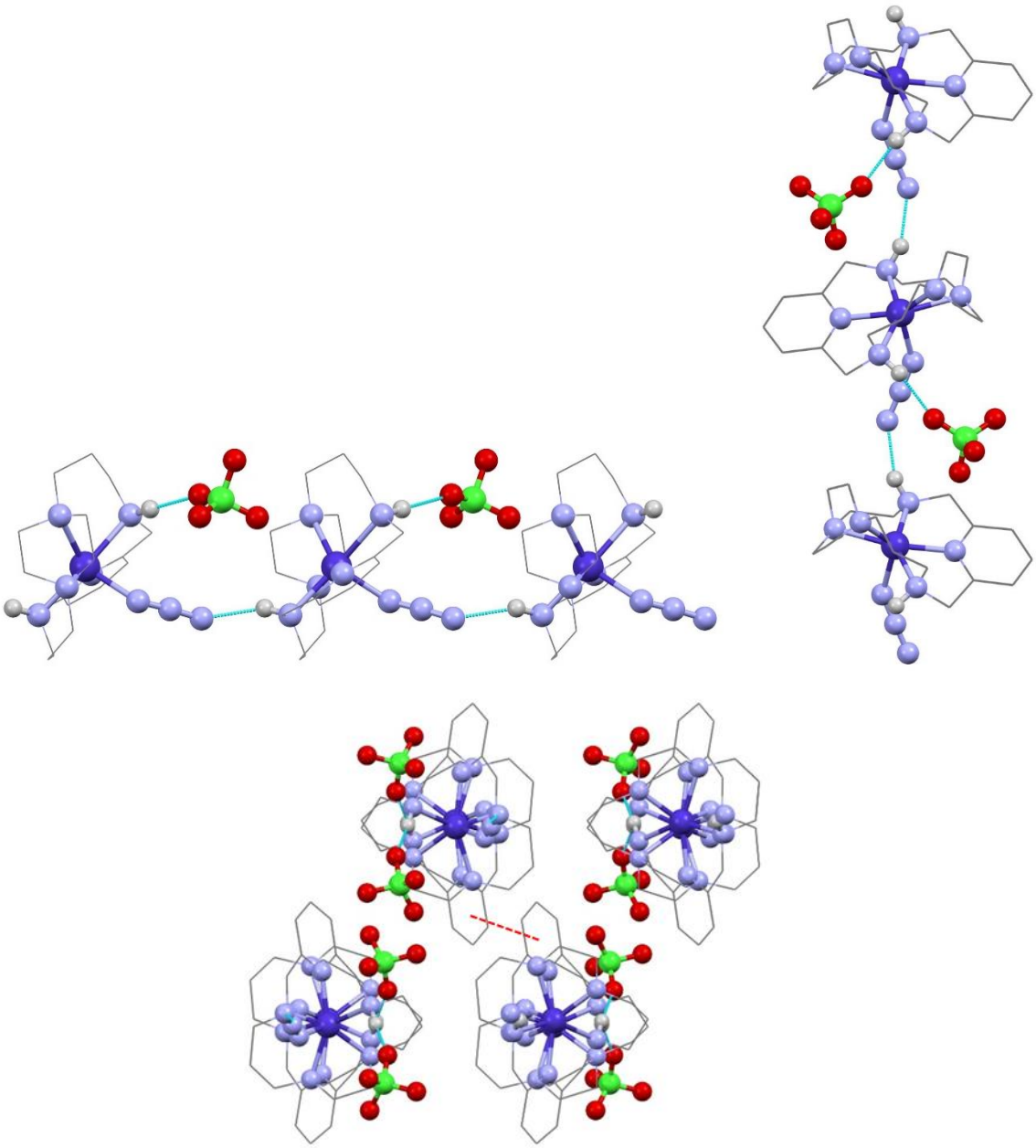

Figure S6 The crystal packing of complex [Co**L**(N_3)]ClO_4 (**3**). View of the supramolecular 1D chain along a axis (*top left*), along c axis (top *left*) and view along b axis (*bottom*). Blue dashed lines represent hydrogen bonds and red dashed lines represent π-π stacking interaction.

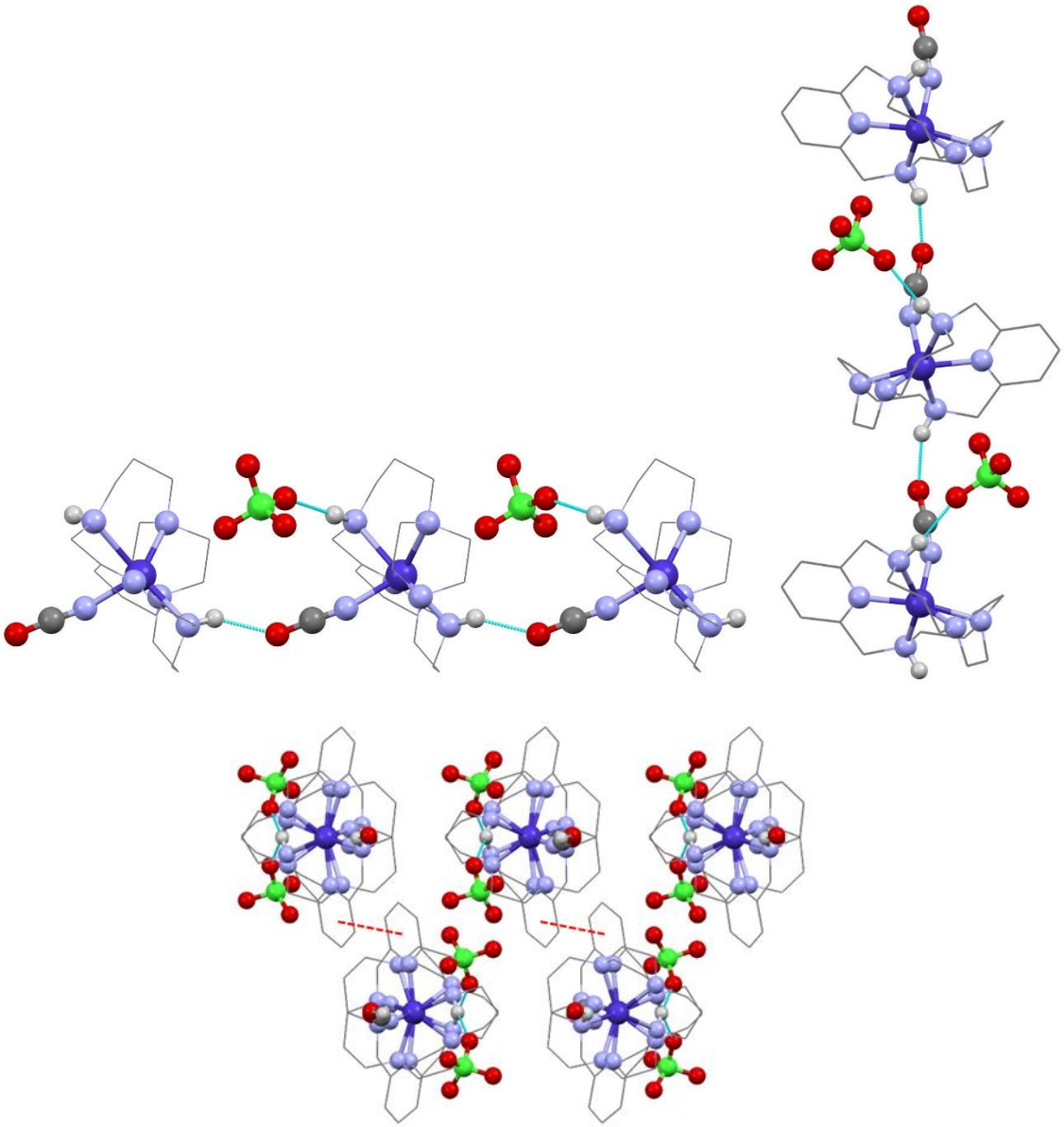

Figure S7 The crystal packing of complex [Co**L**(NCO)]ClO_4 (**4**). View of the supramolecular 1D chain along a axis (*top left*), along c axis (top *left*) and view along b axis (*bottom*). Blue dashed lines represent hydrogen bonds and red dashed lines represent π-π stacking interaction.

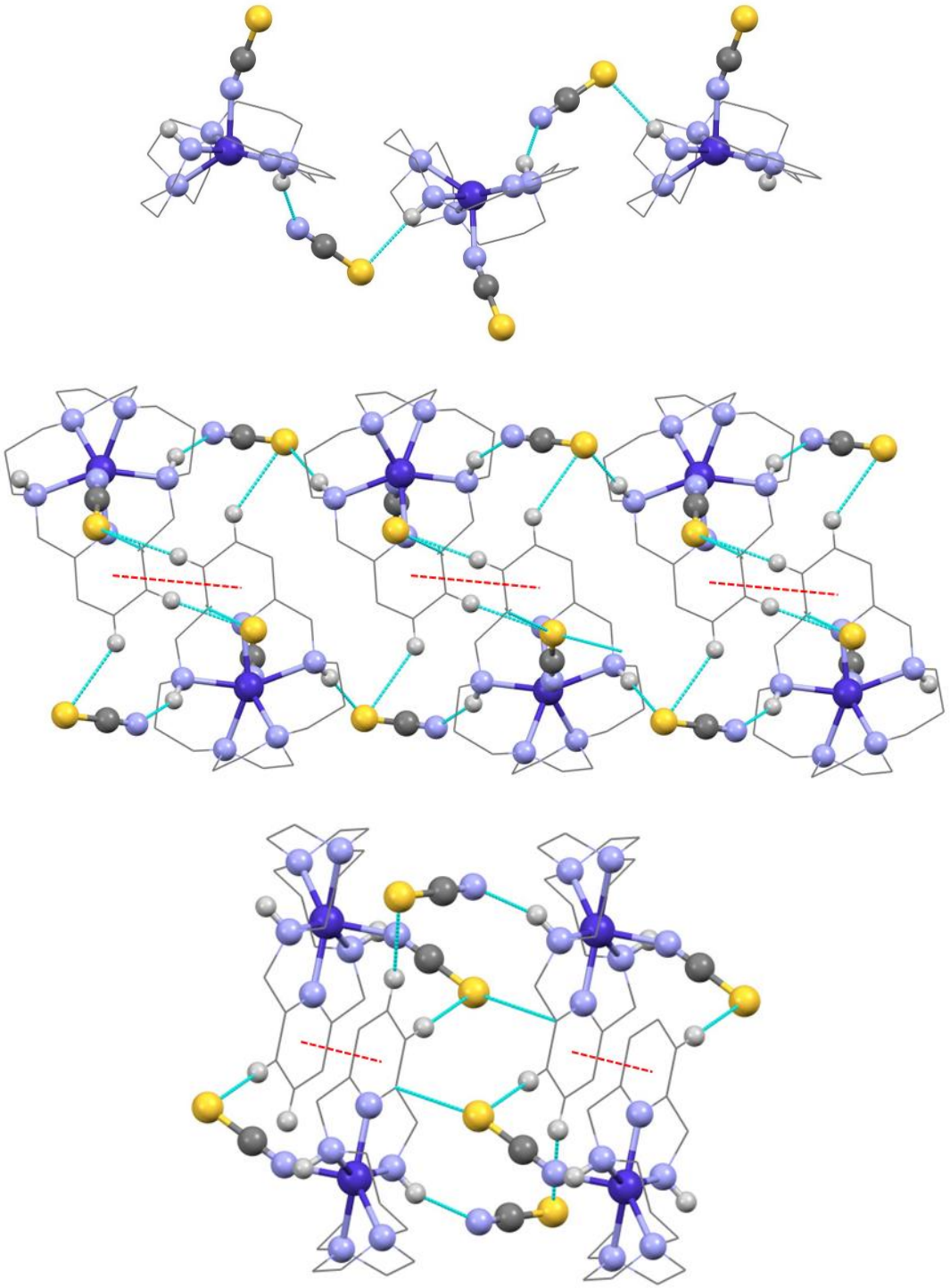

Figure S8 The crystal packing of complex [Co**L**(SCN)]SCN (**5**). View of the supramolecular 1D chain along c axis (*top*), connection between these 1D chains along b axis (*middle*) and better view on these non-covalent contacts (*bottom*). Blue dashed lines represent hydrogen bonds and red dashed lines represent π-π stacking interaction.

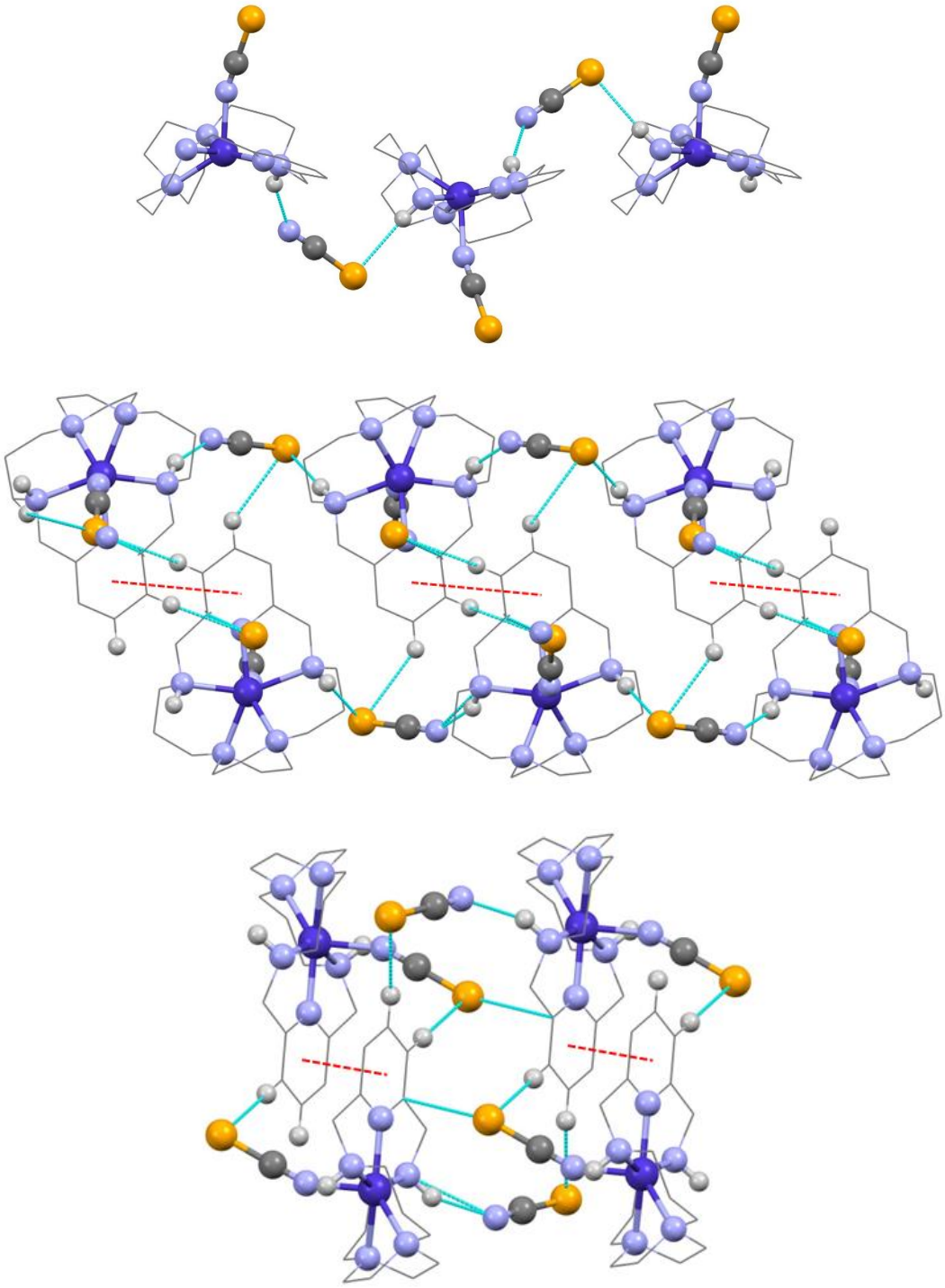

Figure S9 The crystal packing of complex [Co**L**(SeCN)]SeCN (**6**). View of the supramolecular 1D chain along c axis (*top*), connection between these 1D chains along b axis (*middle*) and better view on these non-covalent contacts (*bottom*). Blue dashed lines represent hydrogen bonds and red dashed lines represent π-π stacking interaction.

1a

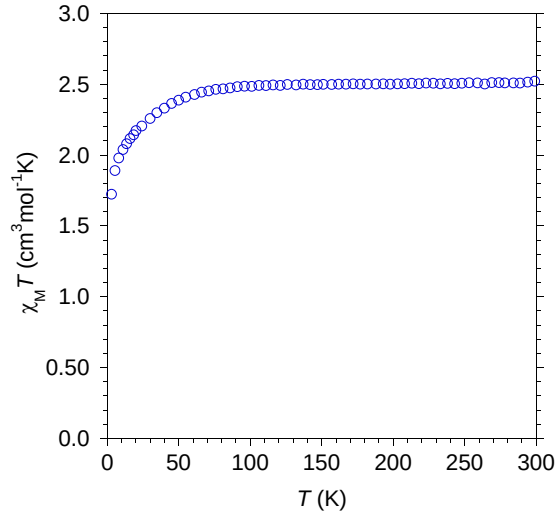
3.0
2.5
2.0
1.5
1.0
0.50
0.0
0
50
100
150
200
250
300
$\chi_M T$ (cm^{3}mol^{-1}K)
T (K)

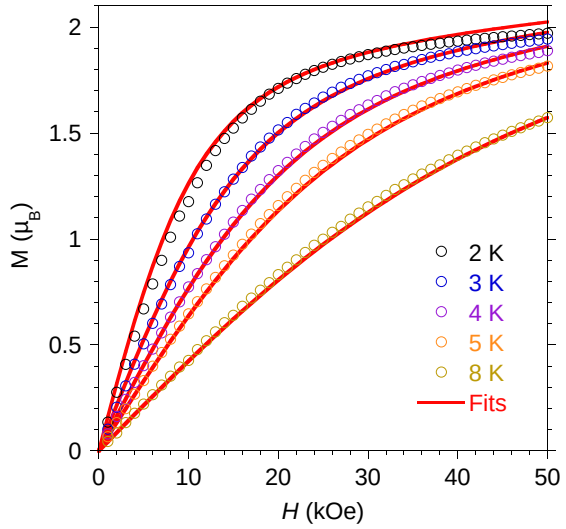
2
1.5
1
0.5
0
0
10
20
30
40
50
M (μ_B)
H (kOe)
2 K
3 K
4 K
5 K
8 K
Fits

1b

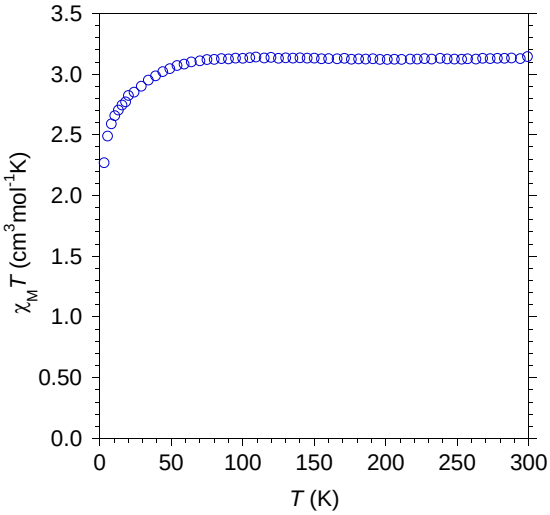
3.5
3.0
2.5
2.0
1.5
1.0
0.50
0.0
0
50
100
150
200
250
300
$\chi_M T$ (cm^{3}mol^{-1}K)
T (K)

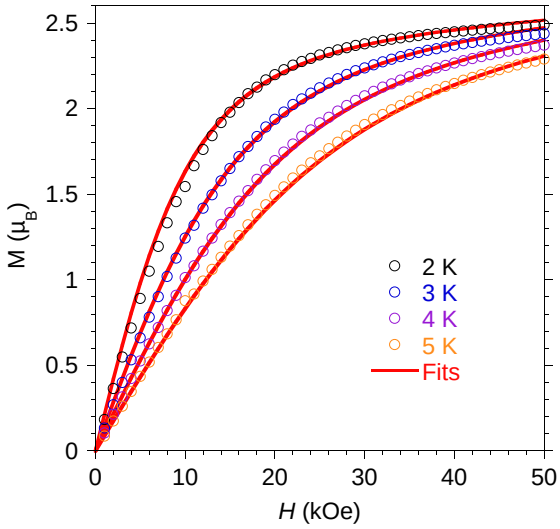
2.5
2
1.5
1
0.5
0
0
10
20
30
40
50
M (μ_B)
H (kOe)
2 K
3 K
4 K
5 K
Fits

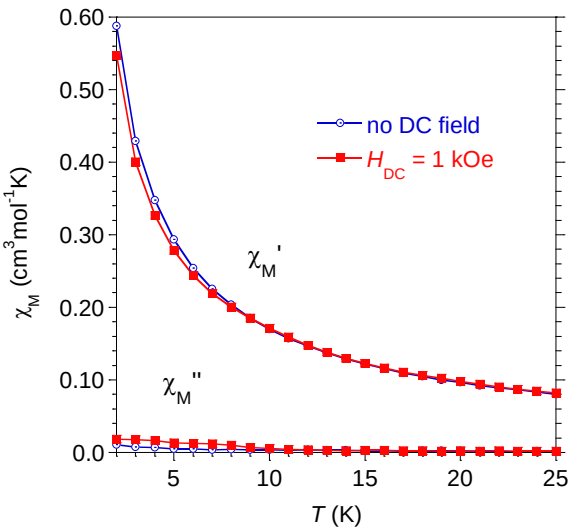
0.60
0.50
0.40
0.30
0.20
0.10
0.0
5
10
15
20
25
χ_M (cm^{3}mol^{-1}K)
T (K)
no DC field
H_{DC} = 1 kOe
χ_M'
χ_M''

Figure S10 Magnetic behaviors for [Co**L**Cl]Cl, **1a,b**. Experimental (O) $\chi_M T = f(T)$ and $M = f(H)$ behaviors, best-fit (–) parameters are given in the plots, and AC susceptibility traces for **1a** without and with applied static field.

AC susceptibility obtained for **1a** in the absence (in blue) and with applied field (1 kOe, in red) with H_{AC} = 3 Oe, and a test frequency of 997 Hz.

(a)

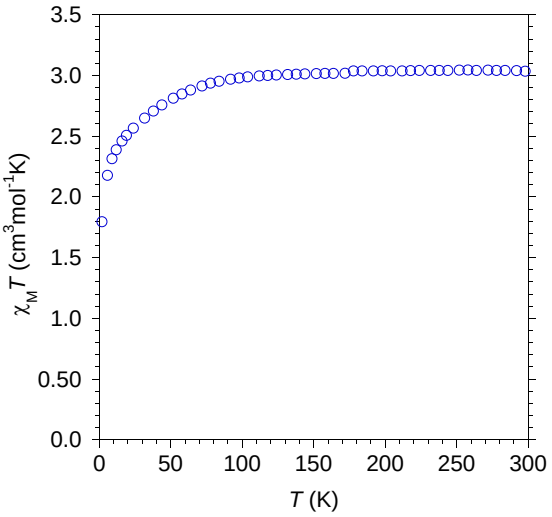
3.5
3.0
2.5
2.0
1.5
1.0
0.50
0.0
0
50
100
150
200
250
300
T (K)
χM T (cm3mol-1K)

(b)

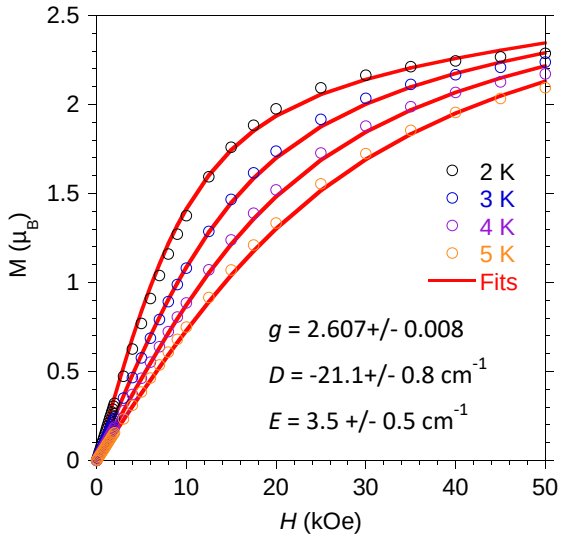
2.5
2
1.5
1
0.5
0
0
10
20
30
40
50
H (kOe)
M (μB)
2 K
3 K
4 K
5 K
Fits
g = 2.607+/- 0.008
D = -21.1+/- 0.8 cm-1
E = 3.5 +/- 0.5 cm-1

(c)

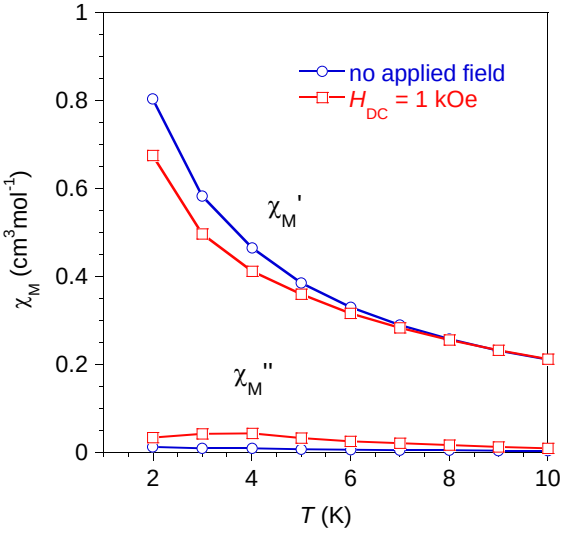
1
0.8
0.6
0.4
0.2
0
2
4
6
8
10
T (K)
χM (cm3mol-1)
no applied field
HDC = 1 kOe
χM'
χM''

(d)

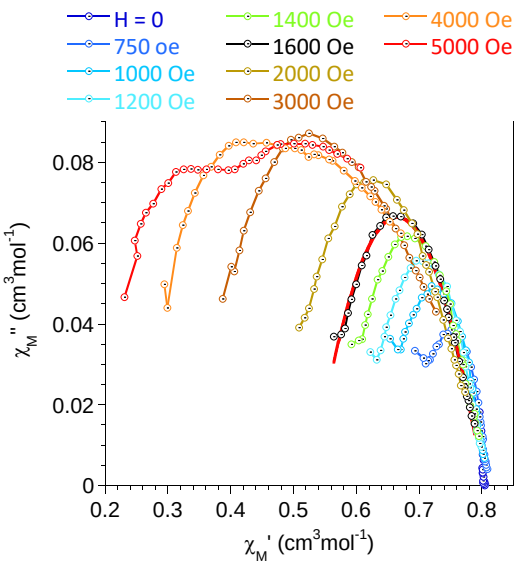
H = 0
750 oe
1000 Oe
1200 Oe
1400 Oe
1600 Oe
2000 Oe
3000 Oe
4000 Oe
5000 Oe
0.08
0.06
0.04
0.02
0
0.2
0.3
0.4
0.5
0.6
0.7
0.8
χM' (cm3mol-1)
χM'' (cm3mol-1)

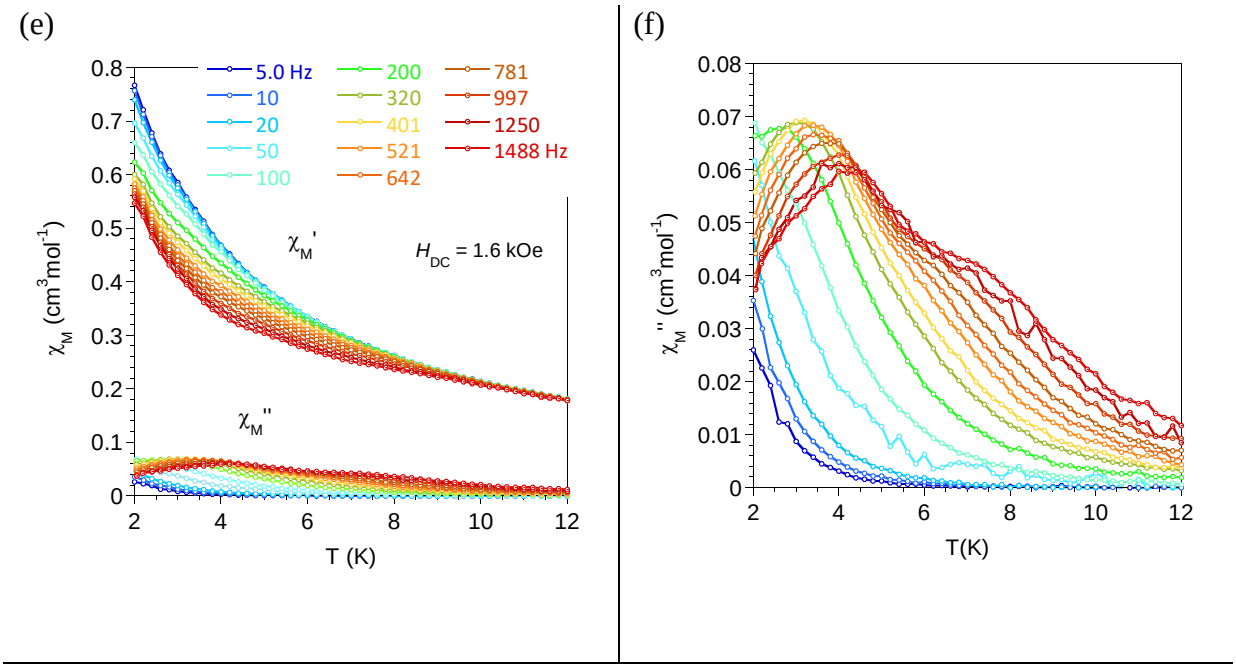

Figure S11 Magnetic behaviors for [Co**L**Br]Br, **2**. (a, b) Experimental (O) and calculated (–) $\chi_M T = f(T)$ and M = $f(H)$ behaviors, best-fit parameters are given in the plot, (c) AC susceptibility traces without and with applied static field(H_{AC} = 3 Oe, test frequency: 997 Hz); (d) $\chi_M'' = f(\chi_M')$ at 2 K for different applied static fields; (e,f) χ_M' and $\chi_M'' = f$(T) for frequencies between 1 and 1488 Hz with H_{DC} = 1.6 kOe.

The field dependence of the AC susceptibility components showed an increase of the χ_M'' signal but revealed also the emergence of a second relaxation process as H_{DC} became larger (4d). A modeling of the $\chi_M'' = f(\chi_M')$ with a gaussian function was possible for applied fields up to 1.6 kOe (red solid line in 4c) therefore this field was considered as optimal for the subsequent investigations.

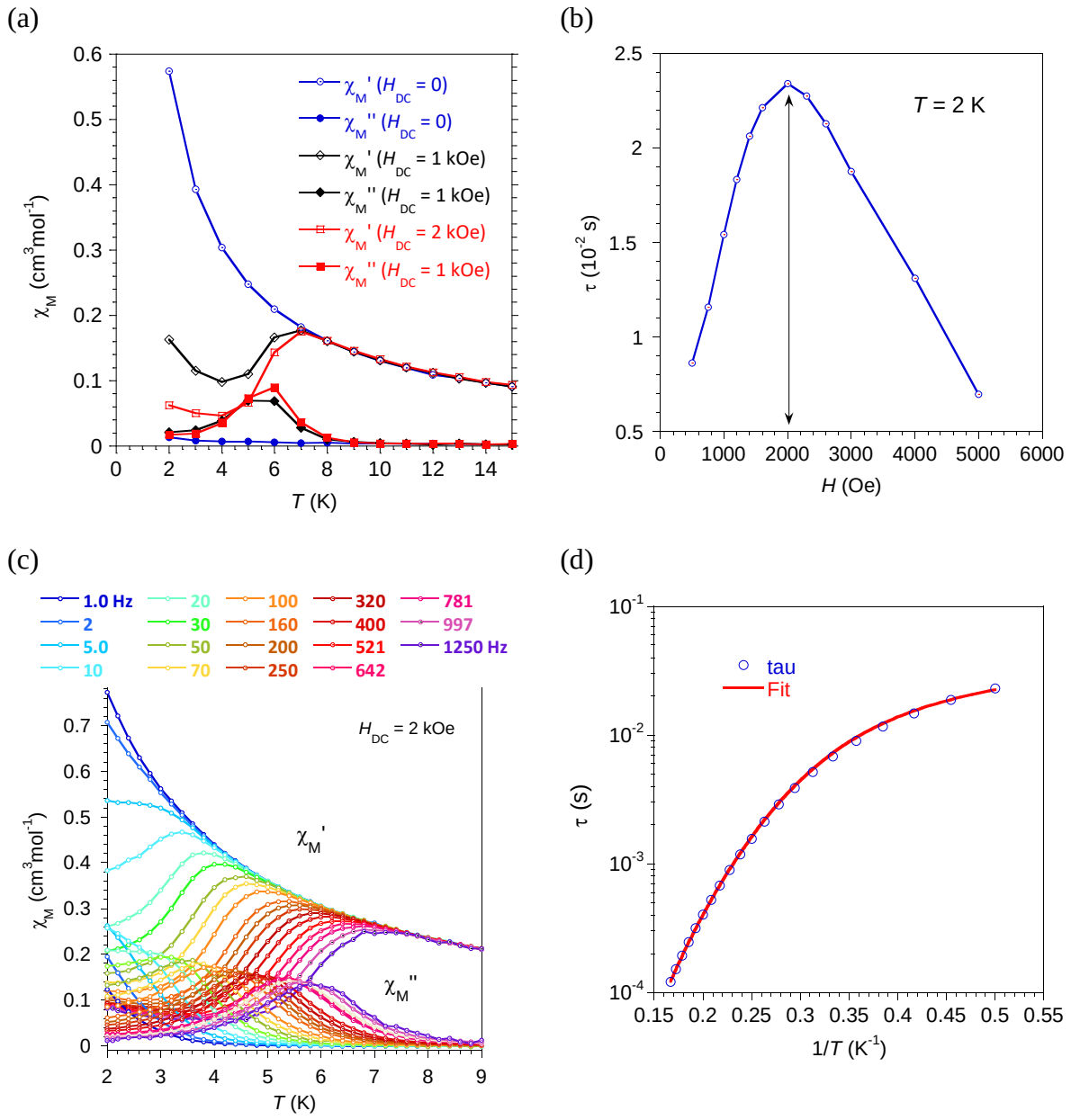

Figure S12 Magnetic behaviors for [Co**L**(N_3)]ClO_4, **3**. (a) AC susceptibility traces without and with applied static field(H_{AC} = 3 Oe, test frequency: 997 Hz); (b) $\tau = f(H_{DC})$ at 2 k; (c) χ_M' and χ_M'' = *f*(T) for frequencies between 1 and 1488 Hz; (d) $\tau = f(1/T)$ with best fit (red line) of relaxation model comprising the Raman and direct expressions.

(a)

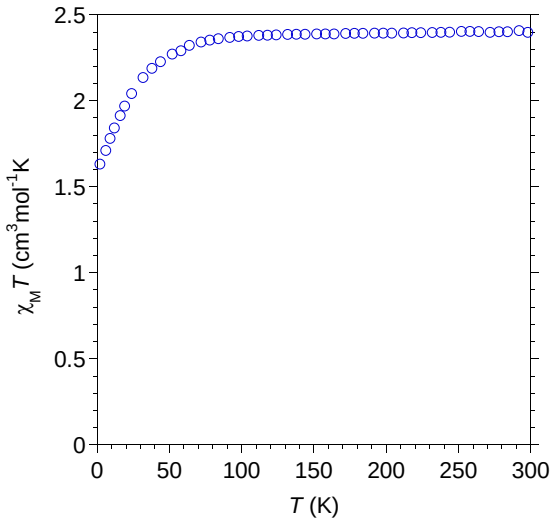
2.5
2
1.5
1
0.5
0
0
50
100
150
200
250
300
T (K)
χM T (cm3mol-1K

(b)

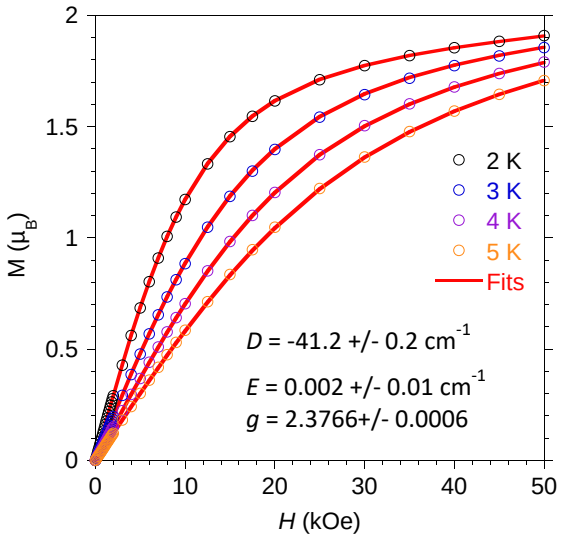
2
1.5
1
0.5
0
0
10
20
30
40
50
H (kOe)
M (μB)
2 K
3 K
4 K
5 K
Fits
D = -41.2 +/- 0.2 cm-1
E = 0.002 +/- 0.01 cm-1
g = 2.3766+/- 0.0006

(c)

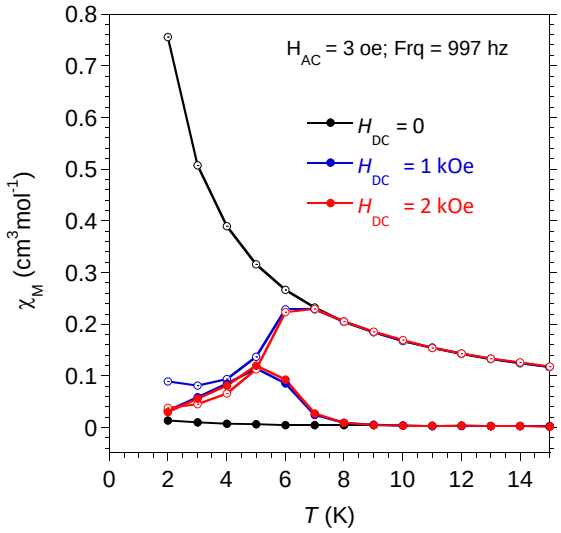
0.8
0.7
0.6
0.5
0.4
0.3
0.2
0.1
0
0
2
4
6
8
10
12
14
T (K)
χM (cm3mol-1)
HAC = 3 oe; Frq = 997 hz
HDC = 0
HDC = 1 kOe
HDC = 2 kOe

(d)

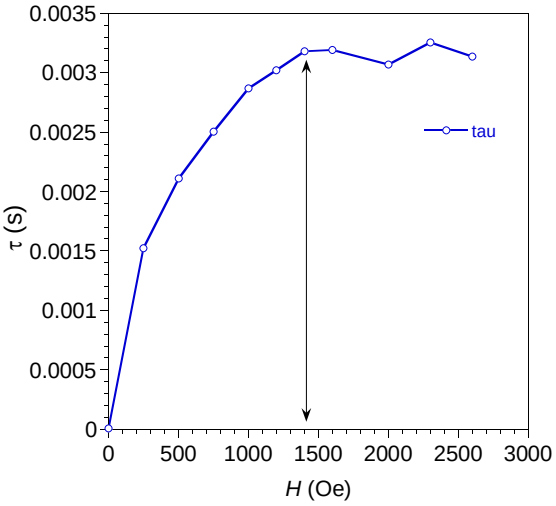
0.0035
0.003
0.0025
0.002
0.0015
0.001
0.0005
0
0
500
1000
1500
2000
2500
3000
H (Oe)
τ (s)
tau

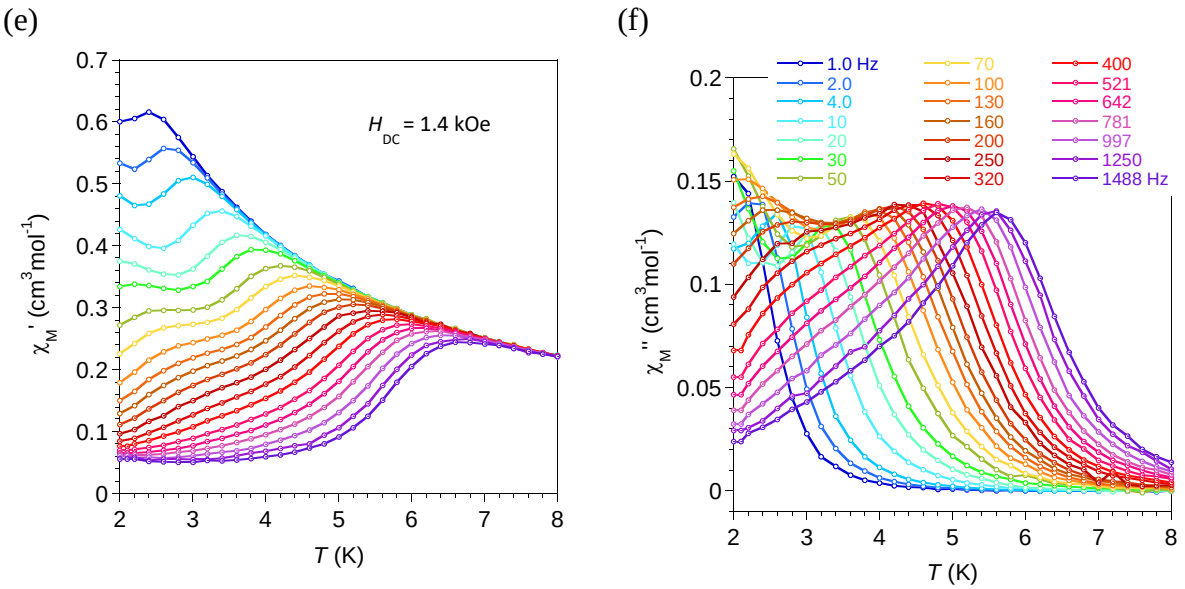

Figure S13 Magnetic behaviors for [Co**L(**NCO)]ClO_4, **4**. (a, b) Experimental (O) and calculated (–) $\chi_M T = f(T)$ and $M = f(H)$ behaviors, best-fit parameters are given in the plot, (c) AC susceptibility traces without and with applied static field (H_{AC} = 3 Oe, test frequency: 997 Hz); (d) $\tau = f(H_{DC})$ at 2 K; (e,f) χ_M' and χ_M'' = *f*(T) for frequencies between 1 and 1488 Hz.

(a)

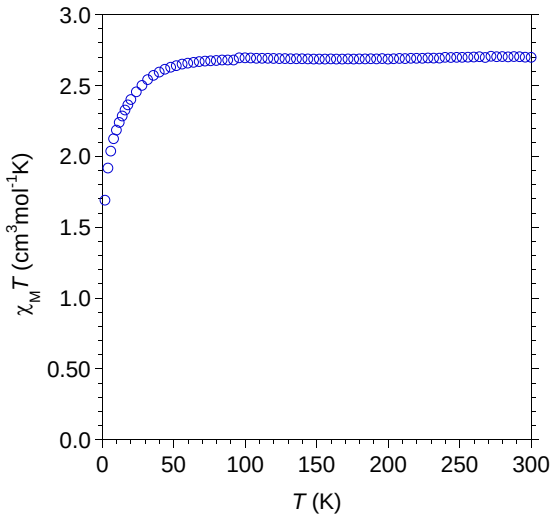
3.0
2.5
2.0
1.5
1.0
0.50
0.0
0
50
100
150
200
250
300
T (K)
χM T (cm3mol-1K)

(b)

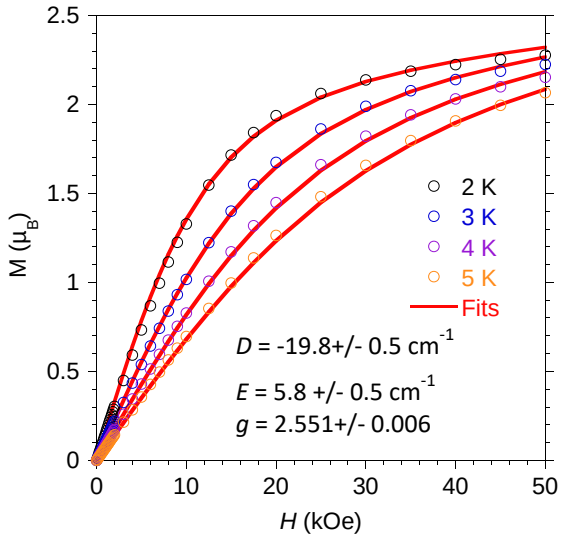
2.5
2
1.5
1
0.5
0
0
10
20
30
40
50
H (kOe)
M (μB)
2 K
3 K
4 K
5 K
Fits
D = -19.8+/- 0.5 cm-1
E = 5.8 +/- 0.5 cm-1
g = 2.551+/- 0.006

(c)

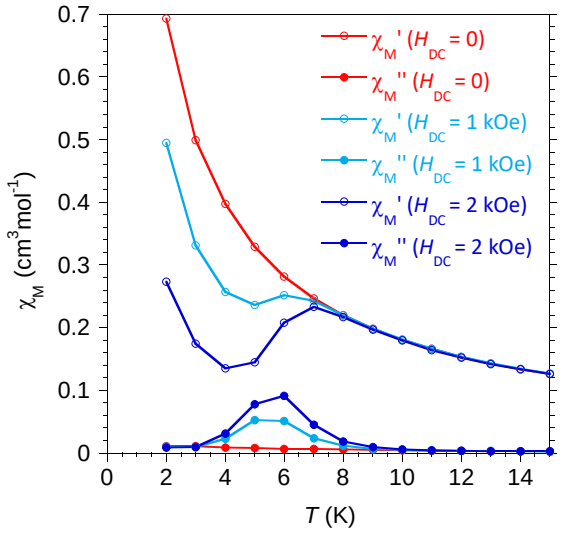
0.7
0.6
0.5
0.4
0.3
0.2
0.1
0
0
2
4
6
8
10
12
14
T (K)
χM (cm3mol-1)
χM' (HDC = 0)
χM'' (HDC = 0)
χM' (HDC = 1 kOe)
χM'' (HDC = 1 kOe)
χM' (HDC = 2 kOe)
χM'' (HDC = 2 kOe)

(d)

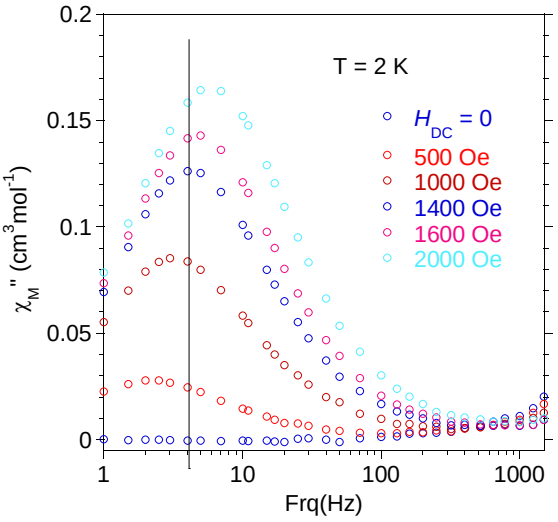
0.2
0.15
0.1
0.05
0
1
10
100
1000
Frq(Hz)
χM'' (cm3mol-1)
T = 2 K
HDC = 0
500 Oe
1000 Oe
1400 Oe
1600 Oe
2000 Oe

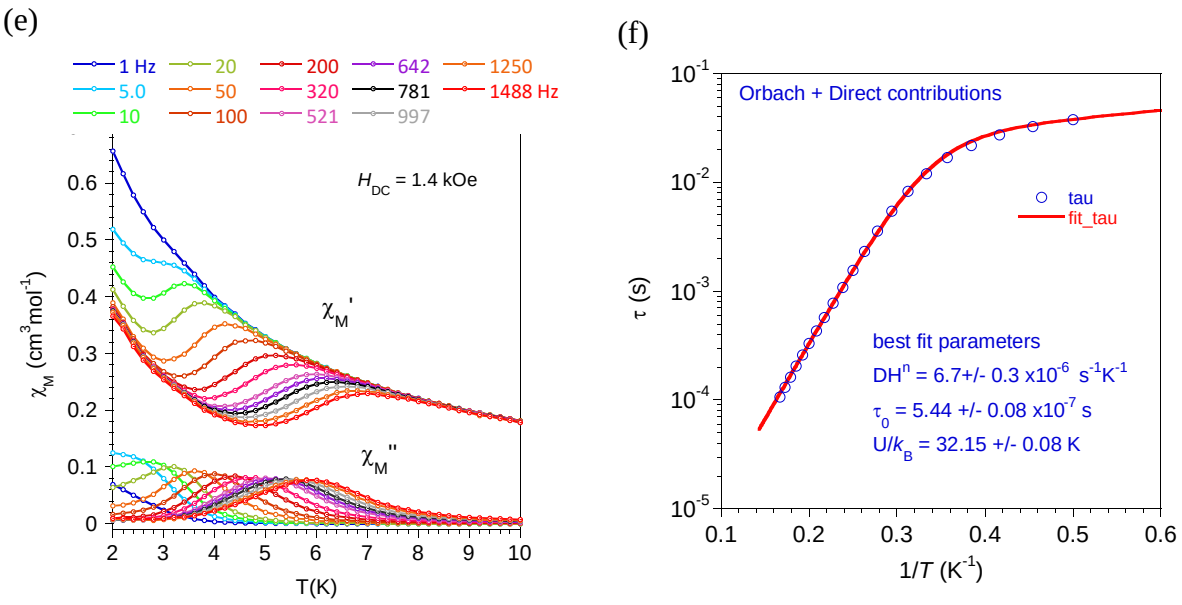

Figure S14 Magnetic behaviors for [Co**L**(NCS)]NCS, **5**: (a, b) Experimental (O) and calculated (–) $\chi_M T = f(T)$ and $M = f(H)$ behaviors, best-fit parameters are given in the plot, (c) AC susceptibility traces without and with applied static field (H_{AC} = 3 Oe, test frequency: 997 Hz); (d) $\chi_M'' = f(H_{DC})$ at 2 K; (e) χ_M' and $\chi_M'' = f$(T) for frequencies between 1 and 1488 Hz; (f) $\tau = f(1/T)$ with best fit (red line) of relaxation model considering the Arrhenius and direct expressions.

(a)

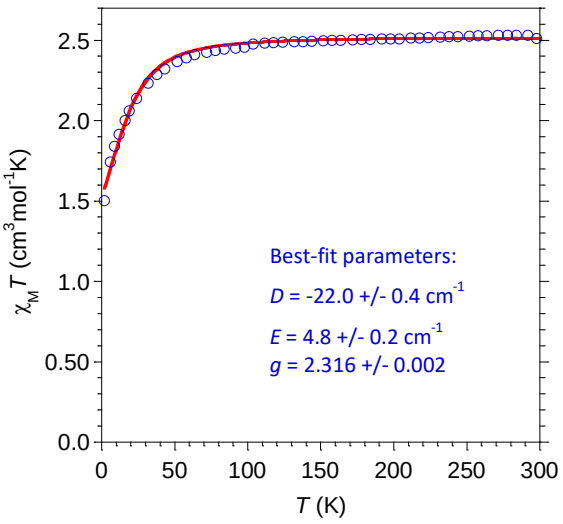
Best-fit parameters:
D = -22.0 +/- 0.4 cm-1
E = 4.8 +/- 0.2 cm-1
g = 2.316 +/- 0.002
χM T (cm3mol-1K)
T (K)

(b)

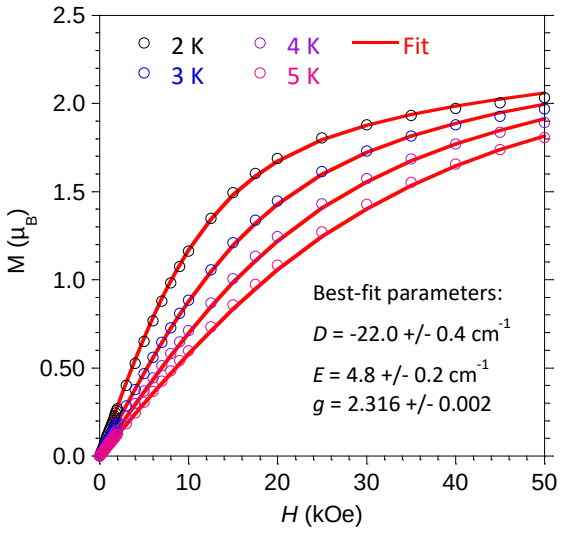
2 K
3 K
4 K
5 K
Fit
Best-fit parameters:
D = -22.0 +/- 0.4 cm-1
E = 4.8 +/- 0.2 cm-1
g = 2.316 +/- 0.002
M (μB)
H (kOe)

(c)

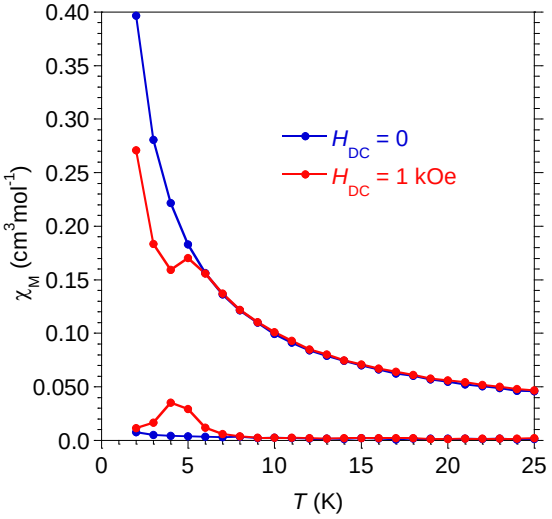
HDC = 0
HDC = 1 kOe
χM (cm3mol-1)
T (K)

(d)

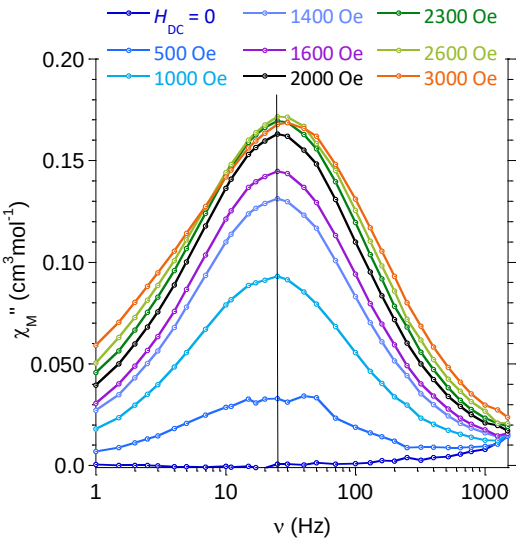
HDC = 0
500 Oe
1000 Oe
1400 Oe
1600 Oe
2000 Oe
2300 Oe
2600 Oe
3000 Oe
χM '' (cm3mol-1)
ν (Hz)

(e)

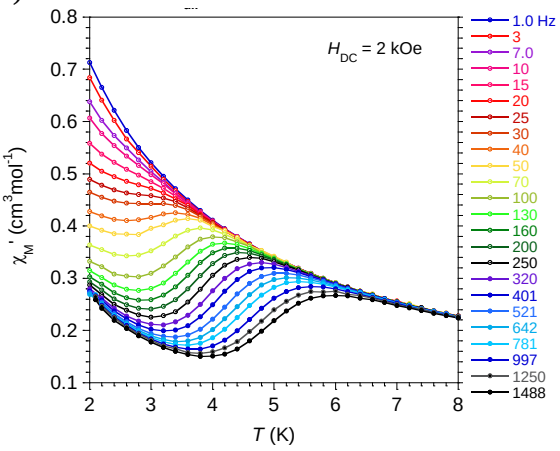
HDC = 2 kOe
1.0 Hz
3
7.0
10
15
20
25
30
40
50
70
100
130
160
200
250
320
401
521
642
781
997
1250
1488
χM ' (cm3mol-1)
T (K)

(f)

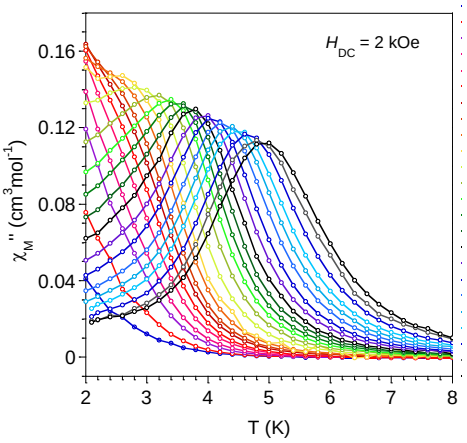
HDC = 2 kOe
χM '' (cm3mol-1)
T (K)

(g)

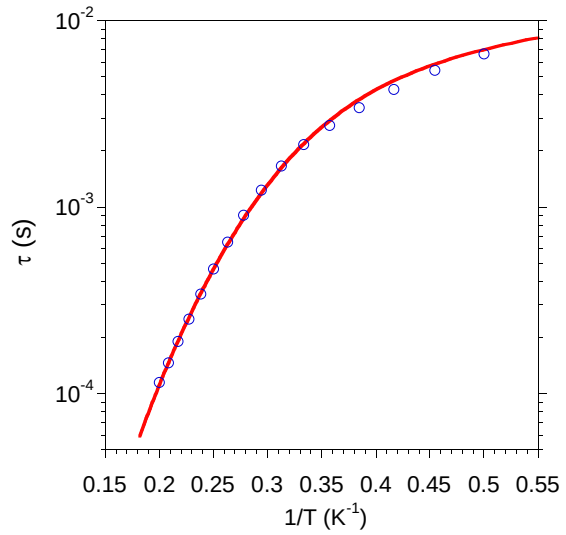

Figure S15 Magnetic behaviors for [Co**L(**NCSe)]NCSe, **6**: (a, b) Experimental (O) and calculated (–) $\chi_M T = f(T)$ and M = $f(H)$ behaviors, best-fit parameters are given in the plot, (c) AC susceptibility traces without and with applied static field (H_{AC} = 3 Oe, test frequency: 997 Hz); (d) $\chi_M'' = f(H_{DC})$ at 2 K; (e,f) χ_M' and $\chi_M'' = f(T)$ for frequencies between 1 and 1488 Hz; (g) $\tau = f(1/T)$ with best fit (red line) of model considering the Raman and direct relaxations expressions.

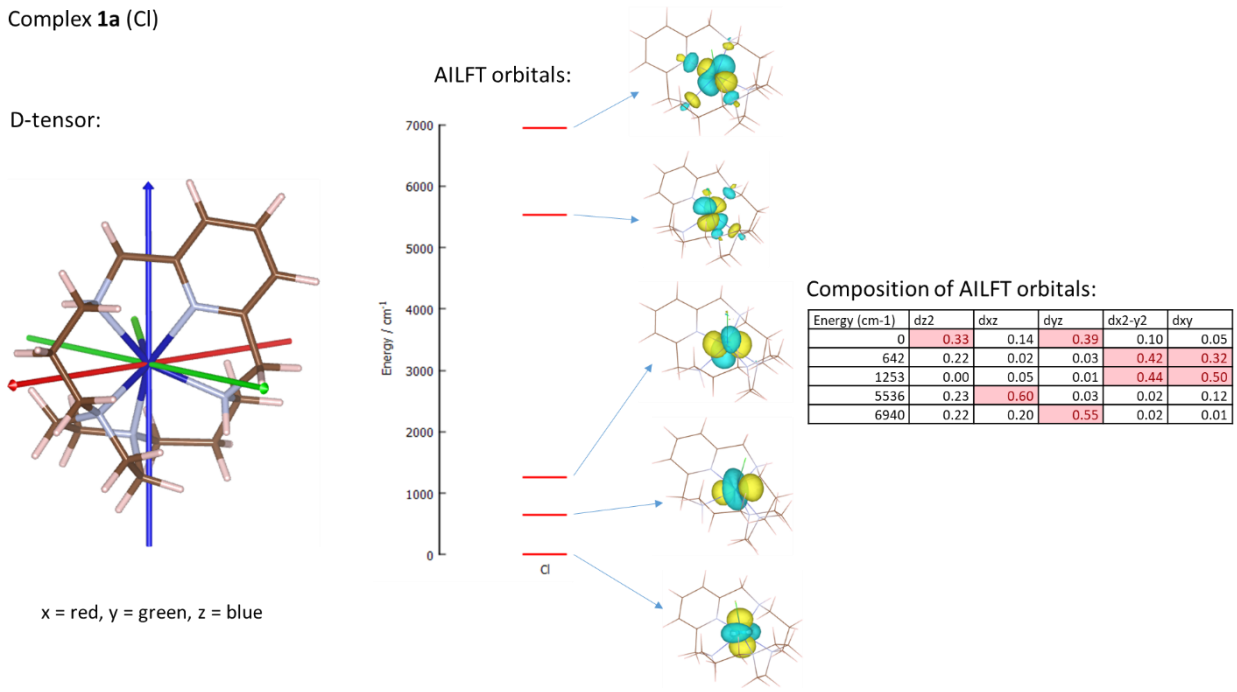

Energy (cm-1)	dz2	dxz	dyz	dx2-y2	dxy
0	0.33	0.14	0.39	0.10	0.05
642	0.22	0.02	0.03	0.42	0.32
1253	0.00	0.05	0.01	0.44	0.50
5536	0.23	0.60	0.03	0.02	0.12
6940	0.22	0.20	0.55	0.02	0.01

Figure S16 Results of the CASSCF/NEVPT2 calculations for the complex **1a** showing (i) the molecular fragment $[Co(L)X]^+$ derived from the experimental X-ray geometries used for CASSCF/NEVPT2 calculations overlaid with the principal axes of the *D*-tensor (x/y/z-axes coloured as red/green/blue arrows) (*left*), (ii) the d-orbital splitting calculated by *ab initio* ligand field theory (AILFT) together with their visualization (utilizing VESTA software) (*middle*), composition of *ab initio* ligand field orbitals centered on Co(II) obtained from CASSCF/NEVPT2 calculations (*right*).

Complex **1b** (Cl)

D-tensor:

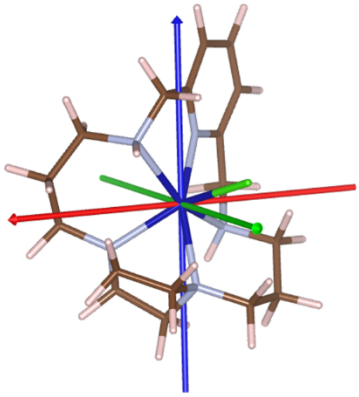

x = red, y = green, z = blue

AILFT orbitals:

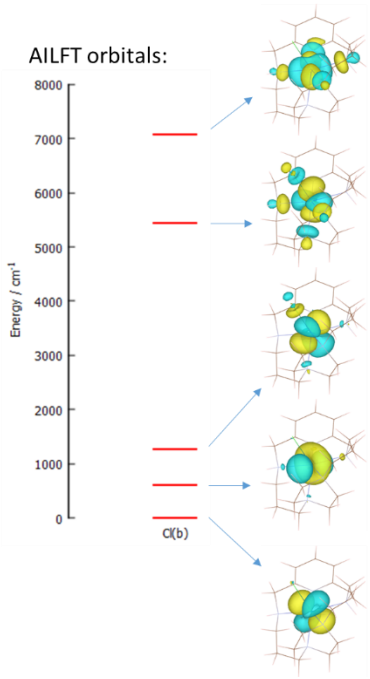

Composition of AILFT orbitals:

Energy (cm-1)	dz2	dxz	dyz	dx2-y2	dxy
0	0.29	0.11	0.46	0.05	0.09
615	0.22	0.02	0.03	0.27	0.47
1283	0.00	0.04	0.01	0.64	0.31
5437	0.30	0.47	0.09	0.01	0.12
7065	0.19	0.37	0.42	0.02	0.01

Figure S17 Results of the CASSCF/NEVPT2 calculations for the complex **1b** showing (i) the molecular fragment $[Co(L)X]^+$ derived from the experimental X-ray geometries used for CASSCF/NEVPT2 calculations overlaid with the principal axes of the *D*-tensor (x/y/z-axes coloured as red/green/blue arrows) (*left*), (ii) the d-orbital splitting calculated by *ab initio* ligand field theory (AILFT) together with their visualization (utilizing VESTA software) (*middle*), composition of *ab initio* ligand field orbitals centered on Co(II) obtained from CASSCF/NEVPT2 calculations (*right*).

Complex **2** (Br(1))

D-tensor:

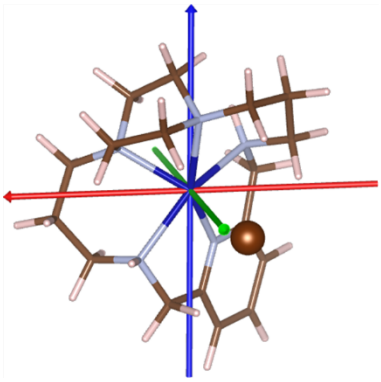

x = red, y = green, z = blue

AILFT orbitals:

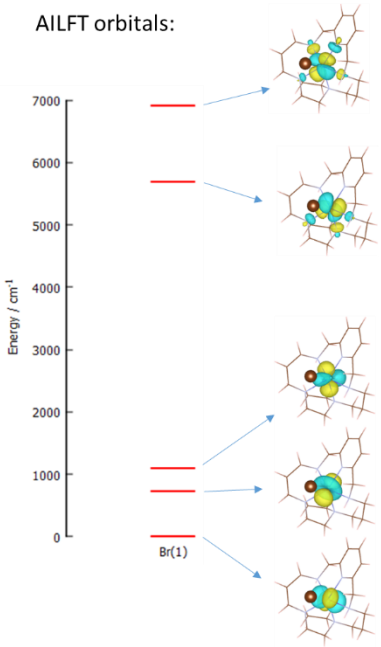

Composition of AILFT orbitals:

Energy (cm-1)	dz2	dxz	dyz	dx2-y2	dxy
0	0.29	0.10	0.44	0.09	0.09
731	0.23	0.00	0.03	0.45	0.28
1106	0.00	0.04	0.01	0.42	0.53
5687	0.34	0.41	0.14	0.02	0.09
6914	0.13	0.45	0.39	0.02	0.01

Figure S18 Results of the CASSCF/NEVPT2 calculations for the complex **2** (first crystallographically independent molecule in the asymmetric unit) showing (i) the molecular fragment $[Co(L)X]^+$ derived from the experimental X-ray geometries used for CASSCF/NEVPT2 calculations overlaid with the principal axes of the *D*-tensor (x/y/z-axes coloured as red/green/blue arrows) (*left*), (ii) the d-orbital splitting calculated by *ab initio* ligand field theory (AILFT) together with their visualization (utilizing VESTA software) (*middle*), composition of *ab initio* ligand field orbitals centered on Co(II) obtained from CASSCF/NEVPT2 calculations (*right*).

Complex **2** (Br(2))

D-tensor:

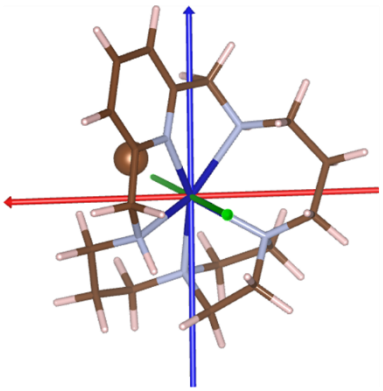

x = red, y = green, z = blue

AILFT orbitals:

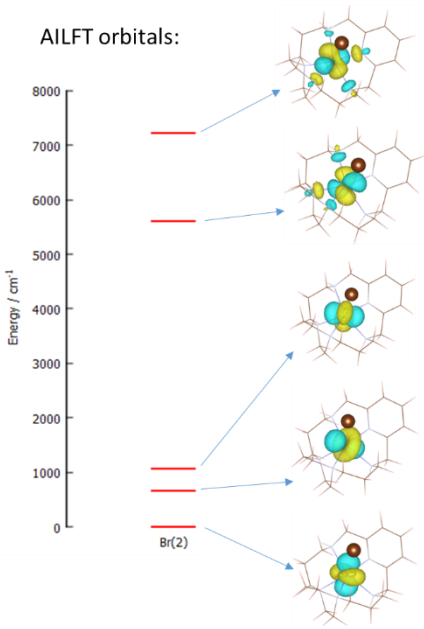

Composition of AILFT orbitals:

Energy (cm-1)	dz2	dxz	dyz	dx2-y2	dxy
0	0.26	0.12	0.46	0.09	0.07
678	0.22	0.01	0.04	0.45	0.29
1073	0.00	0.05	0.01	0.42	0.52
5603	0.26	0.58	0.03	0.01	0.12
7228	0.26	0.25	0.46	0.02	0.00

Figure S19 Results of the CASSCF/NEVPT2 calculations for the complex **2** (second crystallographically independent molecule in the asymmetric unit) showing (i) the molecular fragment $[Co(L)X]^+$ derived from the experimental X-ray geometries used for CASSCF/NEVPT2 calculations overlaid with the principal axes of the *D*-tensor (x/y/z-axes coloured as red/green/blue arrows) (*left*), (ii) the d-orbital splitting calculated by *ab initio* ligand field theory (AILFT) together with their visualization (utilizing VESTA software) (*middle*), composition of *ab initio* ligand field orbitals centered on Co(II) obtained from CASSCF/NEVPT2 calculations (*right*).

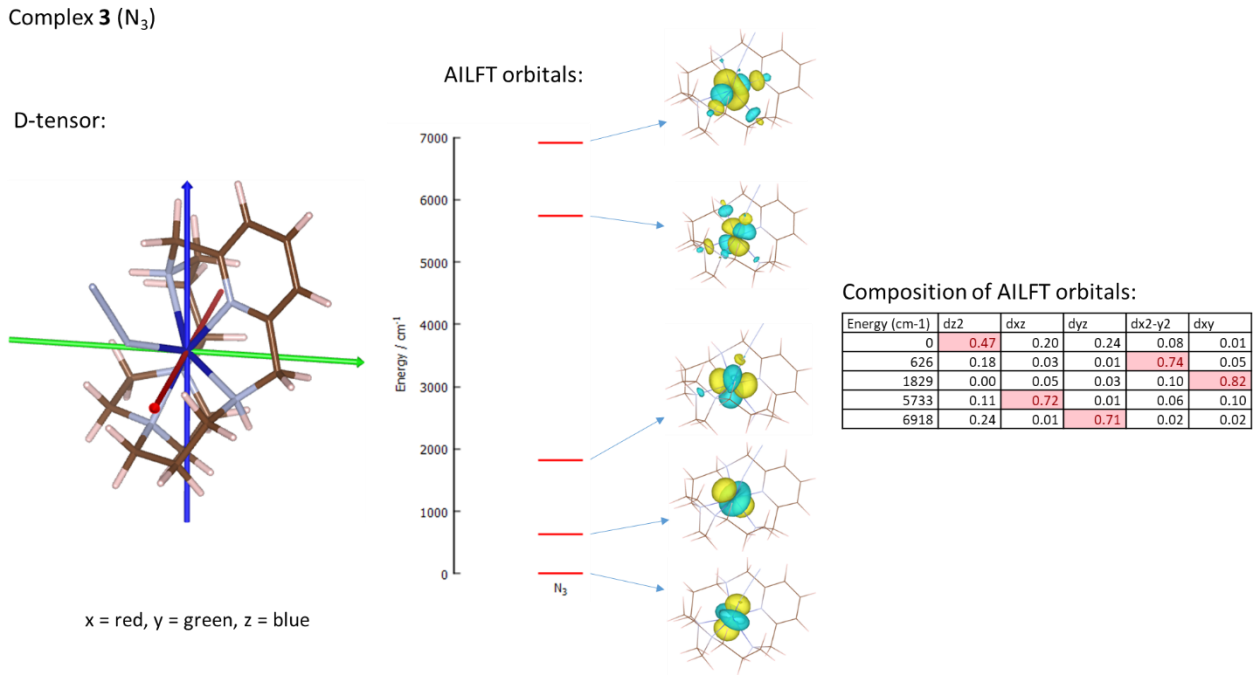

Energy (cm-1)	dz2	dxz	dyz	dx2-y2	dxy
0	0.47	0.20	0.24	0.08	0.01
626	0.18	0.03	0.01	0.74	0.05
1829	0.00	0.05	0.03	0.10	0.82
5733	0.11	0.72	0.01	0.06	0.10
6918	0.24	0.01	0.71	0.02	0.02

Figure S20 Results of the CASSCF/NEVPT2 calculations for the complex **3** showing (i) the molecular fragment $[Co(L)X]^+$ derived from the experimental X-ray geometries used for CASSCF/NEVPT2 calculations overlaid with the principal axes of the *D*-tensor (x/y/z-axes coloured as red/green/blue arrows) (*left*), (ii) the d-orbital splitting calculated by *ab initio* ligand field theory (AILFT) together with their visualization (utilizing VESTA software) (*middle*), composition of *ab initio* ligand field orbitals centered on Co(II) obtained from CASSCF/NEVPT2 calculations (*right*).

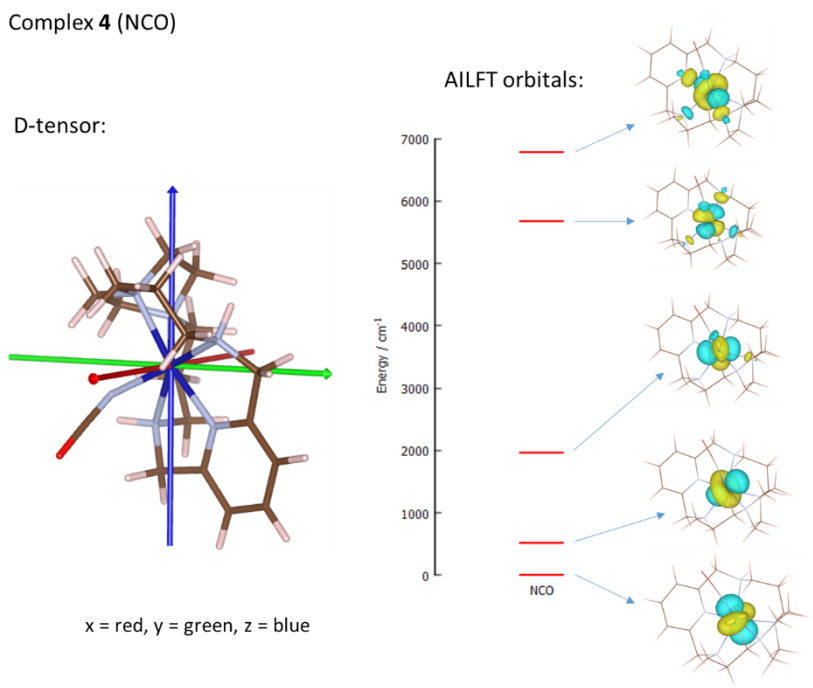

Composition of AILFT orbitals:

Energy (cm-1)	dz2	dxz	dyz	dx2-y2	dxy
0	0.44	0.28	0.13	0.15	0.00
513	0.22	0.01	0.03	0.72	0.02
1973	0.00	0.06	0.05	0.00	0.89
5669	0.06	0.60	0.15	0.11	0.08
6790	0.28	0.05	0.64	0.02	0.01

Figure S21 Results of the CASSCF/NEVPT2 calculations for the complex **4** showing (i) the molecular fragment $[Co(L)X]^+$ derived from the experimental X-ray geometries used for CASSCF/NEVPT2 calculations overlaid with the principal axes of the *D*-tensor (x/y/z-axes coloured as red/green/blue arrows) (*left*), (ii) the d-orbital splitting calculated by *ab initio* ligand field theory (AILFT) together with their visualization (utilizing VESTA software) (*middle*), composition of *ab initio* ligand field orbitals centered on Co(II) obtained from CASSCF/NEVPT2 calculations (*right*).

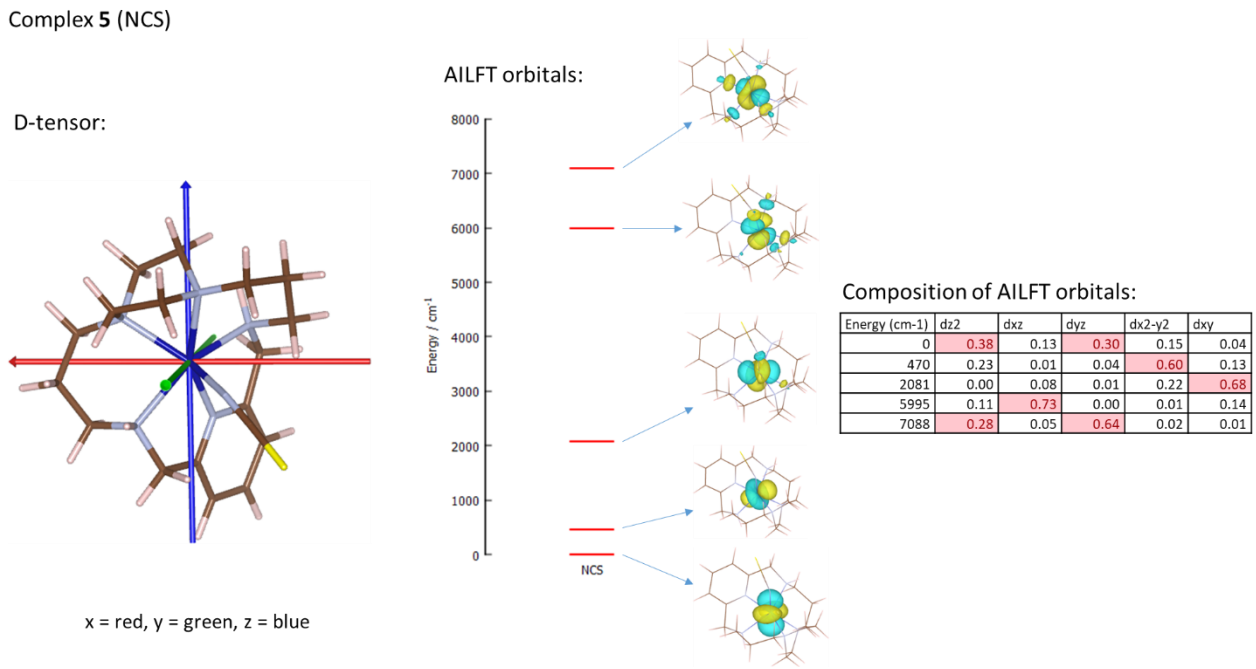

Energy (cm-1)	dz2	dxz	dyz	dx2-y2	dxy
0	0.38	0.13	0.30	0.15	0.04
470	0.23	0.01	0.04	0.60	0.13
2081	0.00	0.08	0.01	0.22	0.68
5995	0.11	0.73	0.00	0.01	0.14
7088	0.28	0.05	0.64	0.02	0.01

Figure S22 Results of the CASSCF/NEVPT2 calculations for the complex **5** showing (i) the molecular fragment $[Co(L)X]^+$ derived from the experimental X-ray geometries used for CASSCF/NEVPT2 calculations overlaid with the principal axes of the *D*-tensor (x/y/z-axes coloured as red/green/blue arrows) (*left*), (ii) the d-orbital splitting calculated by *ab initio* ligand field theory (AILFT) together with their visualization (utilizing VESTA software) (*middle*), composition of *ab initio* ligand field orbitals centered on Co(II) obtained from CASSCF/NEVPT2 calculations (*right*).

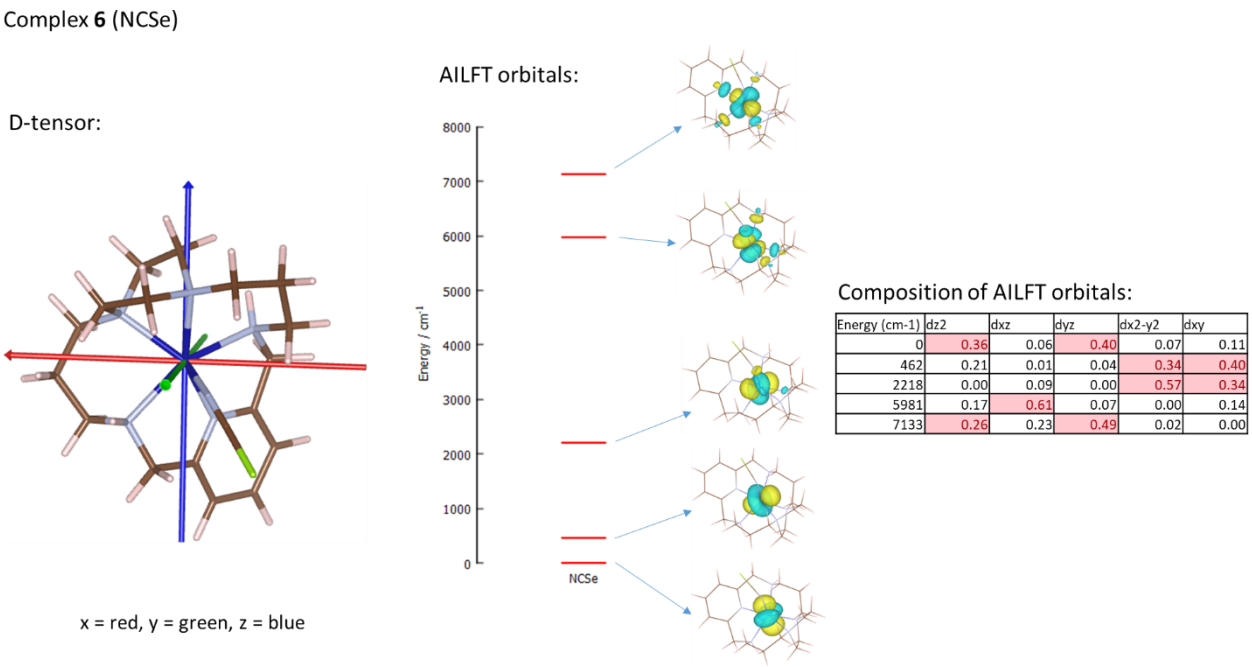

Figure S23 Results of the CASSCF/NEVPT2 calculations for the complex **6** showing (i) the molecular fragment $[Co(L)X]^{+}$ derived from the experimental X-ray geometries used for CASSCF/NEVPT2 calculations overlaid with the principal axes of the *D*-tensor (x/y/z-axes coloured as red/green/blue arrows) (*left*), (ii) the d-orbital splitting calculated by *ab initio* ligand field theory (AILFT) together with their visualization (utilizing VESTA software) (*middle*), composition of *ab initio* ligand field orbitals centered on Co(II) obtained from CASSCF/NEVPT2 calculations (*right*).

Table S1 Results of continuous shape measures calculations using program Shape 2.1 for complexes **1–6**.

	1a	**1b**	**2**		**3**	**4**	**5**	**6**
CN=6[a,b]								
HP-6	30.323	30.269	31.038	30.720	29.210	29.136	28.836	28.792
PPY-6	7.989	7.727	8.481	8.591	6.968	6.927	7.193	6.999
OC-6	12.178	12.580	12.410	12.299	12.894	13.024	12.602	12.865
TPR-6	**4.720**	**4.772**	**4.779**	**4.715**	**5.544**	**5.476**	**5.307**	**5.338**
JPPY-6	12.391	12.158	13.650	13.702	9.715	9.506	9.732	9.487

[a] The listed valued correspond to the deviation between the ideal and real coordination polyhedral, the lowest values are in red color.
[b] HP-6 = hexagon, PPY-6 pentagonal pyramid, OC-6 = octahedron, TPR-6 = trigonal prism, JPPY-6 = Johnson pentagonal pyramid J2.

Table S2 Selected bond angles (°) for the studied complexes **1–6**.

Complex **1a** Angles (°)		Complex **1b** Angles (°)		Complex **2** Angles (°)		Complex **2** Angles (°)	
N1 Co1 Cl1	91.34(8)	N5 Co1 Cl1	106.00(4)	N4 Co1 Br1	86.78(16)	N1A Co2 Br2	89.51(18)
N1 Co1 N5	77.13(9)	N5 Co1 N2	149.78(5)	N4 Co1 N5	78.6(2)	N1A Co2 N2A	76.6(2)
N1 Co1 N2	73.89(9)	N5 Co1 N4	78.93(5)	N4 Co1 N2	132.0(2)	N1A Co2 N5A	74.1(3)
N1 Co1 N3	130.21(10)	N1 Co1 Cl1	90.22(4)	N1 Co1 Br1	90.83(18)	N1A Co2 N3A	153.8(3)
N1 Co1 N4	154.41(11)	N1 Co1 N5	77.17(5)	N1 Co1 N4	152.7(2)	N1A Co2 N4A	130.7(3)
N5 Co1 Cl1	106.11(7)	N1 Co1 N3	131.65(6)	N1 Co1 N5	75.9(2)	N2A Co2 Br2	106.34(18)
N5 Co1 N2	149.70(10)	N1 Co1 N2	73.62(6)	N1 Co1 N3	131.2(3)	N2A Co2 N5A	149.2(2)
N5 Co1 N4	78.91(10)	N1 Co1 N4	154.23(6)	N1 Co1 N2	74.5(2)	N5A Co2 Br2	82.85(18)
N2 Co1 Cl1	83.38(8)	N3 Co1 Cl1	127.78(4)	N5 Co1 Br1	105.45(17)	N3A Co2 Br2	87.9(2)
N3 Co1 Cl1	129.00(7)	N3 Co1 N5	112.05(6)	N5 Co1 N2	149.0(2)	N3A Co2 N2A	79.0(3)
N3 Co1 N5	110.58(10)	N3 Co1 N2	82.64(6)	N3 Co1 Br1	129.95(18)	N3A Co2 N5A	131.3(3)
N3 Co1 N2	82.38(11)	N3 Co1 N4	67.24(6)	N3 Co1 N4	67.3(2)	N4A Co2 Br2	130.28(19)
N3 Co1 N4	67.49(11)	N2 Co1 Cl1	81.93(4)	N3 Co1 N5	109.9(2)	N4A Co2 N2A	110.3(3)
N4 Co1 Cl1	86.73(7)	N4 Co1 Cl1	87.17(4)	N3 Co1 N2	83.5(2)	N4A Co2 N5A	82.5(3)
N4 Co1 N2	131.01(10)	N4 Co1 N2	131.12(6)	N2 Co1 Br1	83.93(17)	N4A Co2 N3A	67.8(3)

Complex **3** Angles (°)		Complex **4** Angles (°)		Complex **5** Angles (°)		Complex **6** Angles (°)	
N1 Co1 N3	131.32(11)	N5 Co1 N2	149.14(10)	N5 Co1 N2	150.77(10)	N1 Co1 N5	76.75(10)
N1 Co1 N2	73.00(10)	N5 Co1 N4	79.74(10)	N5 Co1 N4	79.62(9)	N1 Co1 N3	134.56(12)
N1 Co1 N4	155.03(11)	N1 Co1 N5	76.99(10)	N1 Co1 N5	76.78(9)	N1 Co1 N4	153.34(11)
N1 Co1 N5	77.22(11)	N1 Co1 N2	72.91(9)	N1 Co1 N2	74.58(10)	N1 Co1 N2	74.60(11)
N3 Co1 N2	82.57(11)	N1 Co1 N3	131.19(10)	N1 Co1 N3	133.52(10)	N5 Co1 N4	79.51(10)
N3 Co1 N4	67.18(11)	N1 Co1 N4	155.14(10)	N1 Co1 N4	153.86(10)	N5 Co1 N2	150.81(10)
N3 Co1 N5	113.25(10)	N3 Co1 N5	113.49(10)	N3 Co1 N5	113.63(9)	N3 Co1 N5	114.52(10)
N4 Co1 N2	130.92(10)	N3 Co1 N2	82.45(10)	N3 Co1 N2	82.88(10)	N3 Co1 N4	67.33(11)
N5 Co1 N2	149.46(11)	N3 Co1 N4	67.04(10)	N3 Co1 N4	67.19(10)	N3 Co1 N2	82.71(11)
N5 Co1 N4	79.54(11)	N4 Co1 N2	131.01(10)	N6 Co1 N5	103.38(10)	N4 Co1 N2	129.68(11)
N6 Co1 N1	94.40(13)	N6 Co1 N5	104.57(11)	N6 Co1 N1	90.01(11)	N6 Co1 N1	89.51(12)
N6 Co1 N3	125.74(14)	N6 Co1 N1	92.94(11)	N6 Co1 N2	82.43(10)	N6 Co1 N5	103.14(12)
N6 Co1 N2	86.17(12)	N6 Co1 N2	83.82(11)	N6 Co1 N3	126.99(11)	N6 Co1 N3	126.06(12)
N6 Co1 N4	81.97(12)	N6 Co1 N3	125.97(12)	N6 Co1 N4	84.63(11)	N6 Co1 N4	84.21(12)
N6 Co1 N5	102.86(13)	N6 Co1 N4	84.50(11)	N4 Co1 N2	129.61(10)	N6 Co1 N2	82.16(11)

Table S3 Calculated individual non-zero contributions to *D*-tensor for studied complexes **1**–**6** obtained from the CASSCF/NEVPT2 calculation together with the major contributing electronic configurations (≥10%) corresponding to the computed electronic states (CASSCF; ground and first excited state) as well as contributions to *D*-tensor from transitions between the electronic configurations of the ground and the first excited state by analysis of Lambda tensor (perturbation theory).

Complex 1a (Cl)

Multiplicity		Root	D [cm^{-1}]	E [cm^{-1}]
4		1	-68.735	0.054
4		2	7.231	-6.813
4		3	5.763	2.151
4		4	4.286	2.074
4		5	-0.002	-0.035
4		6	0.019	-0.155
4		7	0.032	-0.027
4		8	-0.037	-0.000
4		9	-0.014	-0.003
2		0	-0.837	-0.088
2		1	0.910	0.067
2		2	0.003	0.003
2		3	0.812	-0.068
2		4	0.239	-0.001
2		5	0.939	-0.011
2		6	3.413	-0.009
2		7	-2.125	1.162
2		8	-2.184	-1.492
2		9	-0.003	0.003
2		10	-0.004	0.020
2		11	-0.036	-0.040
2		12	0.165	0.027
2		13	-0.009	-0.002
2		14	-0.047	0.066
2		15	-0.002	0.013
2		16	0.003	-0.012
2		17	0.186	-0.026
2		18	0.006	0.003
2		19	0.207	-0.017
2		20	-0.338	0.260
2		21	-0.955	-0.447
2		22	-0.384	0.226
2		23	0.068	-0.004
2		24	0.147	0.000
2		25	0.085	-0.012
2		26	0.000	0.000

2		27	0.003	-0.000
2		28	-0.038	-0.089
2		29	-0.004	-0.004
2		30	-0.070	0.074
2		31	0.126	0.026
2		32	0.011	-0.003
2		33	0.021	0.002
2		34	-0.001	0.000
2		35	0.015	-0.001
2		36	-0.010	0.011
2		37	0.023	-0.003
2		38	-0.011	0.012
2		39	-0.017	-0.027

LF term	**CASSCF energy [cm^{-1}]**	**NEVPT2 energy [cm^{-1}]**	**Dominant electronic configurations based on CASSCF orbitals**		**Contribution to D [cm^{-1}]**	**Contribution to E [cm^{-1}]**
ground state	0	0	$d_{z2}^2 d_{xz}^1 d_{yz}^1 d_{x2-y2}^1 d_{xy}^2$ (33%) $d_{z2}^1 d_{xz}^1 d_{yz}^2 d_{x2-y2}^1 d_{xy}^2$ (28%)	a b		
1st excited state	1105.4	1505.4	$d_{z2}^2 d_{xz}^1 d_{yz}^1 d_{x2-y2}^2 d_{xy}^1$ (48%) $d_{z2}^1 d_{xz}^1 d_{yz}^2 d_{x2-y2}^2 d_{xy}^1$ (23%)	c d	-68.735	0.054

transition	**Δm_l**	**Contribution to D**
a → c	0	strong negative
a → d	-	none
b → c	-	none
b → d	0	strong negative

Complex 1b (Cl)

Multiplicity	Root	D [cm^{-1}]	E [cm^{-1}]
4	1	-67.077	0.046
4	2	7.317	-6.704
4	3	5.586	0.838
4	4	4.392	2.828
4	5	0.002	-0.010
4	6	-0.011	-0.124
4	7	0.035	-0.024
4	8	-0.038	0.000
4	9	-0.016	-0.002
2	0	-0.847	-0.037
2	1	0.737	0.055
2	2	0.049	0.003
2	3	0.731	-0.095
2	4	0.116	-0.005
2	5	-0.013	-0.000
2	6	4.623	0.008
2	7	-2.174	0.610
2	8	-2.196	-1.000
2	9	-0.007	-0.003
2	10	0.020	-0.026
2	11	-0.038	-0.116
2	12	0.123	0.024
2	13	0.078	-0.011
2	14	-0.155	0.037
2	15	0.009	0.022
2	16	0.016	-0.016
2	17	0.152	-0.028
2	18	0.072	0.005
2	19	0.176	-0.012
2	20	-0.348	0.193
2	21	-0.922	-0.333
2	22	-0.377	0.186
2	23	0.038	0.006
2	24	0.192	-0.001
2	25	0.066	-0.016
2	26	0.000	-0.000
2	27	0.002	0.000
2	28	-0.047	-0.107
2	29	-0.005	-0.005
2	30	-0.051	0.092
2	31	0.107	0.032
2	32	0.011	-0.001

2	33	0.032	-0.003
2	34	-0.001	0.001
2	35	0.016	-0.001
2	36	-0.009	0.011
2	37	0.021	-0.003
2	38	-0.011	0.010
2	39	-0.020	-0.029

LF term	**CASSCF energy [cm^{-1}]**	**NEVPT2 energy [cm^{-1}]**	**Dominant electronic configurations based on CASSCF orbitals**		**Contribution to D [cm^{-1}]**	**Contribution to E [cm^{-1}]**
ground state	0	0	$d_{z2}^1 d_{xz}^1 d_{yz}^2 d_{x2-y2}^1 d_{xy}^2$ (37%) $d_{z2}^2 d_{xz}^1 d_{yz}^1 d_{x2-y2}^1 d_{xy}^2$ (37%)	a b		
1st excited state	1155.7	1569.0	$d_{z2}^2 d_{xz}^1 d_{yz}^1 d_{x2-y2}^2 d_{xy}^1$ (50%) $d_{z2}^1 d_{xz}^1 d_{yz}^2 d_{x2-y2}^2 d_{xy}^1$ (34%)	c d	-67.077	0.046

transition	**Δm_l**	**Contribution to D**
a → c	-	none
a → d	0	strong negative
b → c	0	strong negative
b → d	-	none

Comples 2 (Br, first asymmetric unit)

Multiplicity	Root	D [cm^{-1}]	E [cm^{-1}]
4	1	-81.484	0.054
4	2	8.126	-7.872
4	3	3.313	-0.439
4	4	5.292	4.890
4	5	0.253	0.191
4	6	0.004	-0.121
4	7	0.037	-0.032
4	8	-0.050	0.000
4	9	-0.014	-0.001
2	0	-0.786	0.056
2	1	0.654	0.101
2	2	0.195	-0.018
2	3	0.422	-0.025
2	4	0.212	0.000
2	5	-0.064	-0.037
2	6	4.832	-0.016
2	7	-2.244	0.928
2	8	-2.208	-1.371
2	9	-0.058	-0.062
2	10	-0.040	0.005
2	11	0.096	-0.067
2	12	0.147	0.006
2	13	-0.104	-0.017
2	14	-0.044	0.040
2	15	-0.023	0.040
2	16	0.040	0.003
2	17	0.062	-0.003
2	18	0.106	-0.001
2	19	0.159	-0.010
2	20	-0.298	0.197
2	21	-0.997	-0.107
2	22	-0.393	-0.098
2	23	0.135	0.004
2	24	0.072	0.000
2	25	0.086	-0.025
2	26	-0.001	-0.002
2	27	0.001	-0.000
2	28	-0.037	-0.101
2	29	-0.006	-0.006
2	30	-0.023	0.072
2	31	0.081	0.040
2	32	0.021	-0.004

2	33	0.025	0.001
2	34	-0.001	0.001
2	35	0.013	-0.001
2	36	-0.011	0.012
2	37	0.021	-0.002
2	38	-0.011	0.010
2	39	-0.019	-0.029

LF term	CASSCF energy [cm^{-1}]	NEVPT2 energy [cm^{-1}]	Dominant electronic configurations based on CASSCF orbitals		Contribution to D [cm^{-1}]	Contribution to E [cm^{-1}]
ground state	0	0	$d_{z2}^2 d_{xz}^1 d_{yz}^1 d_{x2-y2}^1 d_{xy}^2$ (39%) $d_{z2}^1 d_{xz}^1 d_{yz}^2 d_{x2-y2}^1 d_{xy}^2$ (37%)	a b		
1st excited state	905.0	1234.5	$d_{z2}^2 d_{xz}^1 d_{yz}^1 d_{x2-y2}^2 d_{xy}^1$ (53%) $d_{z2}^1 d_{xz}^1 d_{yz}^2 d_{x2-y2}^2 d_{xy}^1$ (32%)	c d	-81.484	0.054

transition	Δm_l	Contribution to D
a → c	0	strong negative
a → d	-	none
b → c	-	none
b → d	0	strong negative

Complex 2 (Br, second asymmetric unit)

Multiplicity	Root	D [cm^{-1}]	E [cm^{-1}]
4	1	-77.598	0.054
4	2	7.359	-6.999
4	3	4.559	0.265
4	4	4.877	3.826
4	5	0.008	0.031
4	6	0.031	-0.182
4	7	0.039	-0.033
4	8	-0.051	0.000
4	9	-0.014	-0.003
2	0	-0.859	0.197
2	1	0.692	-0.022
2	2	-0.013	-0.006
2	3	0.777	-0.070
2	4	0.278	0.004
2	5	2.143	-0.002
2	6	2.290	-0.026
2	7	-2.139	1.048
2	8	-2.222	-1.562
2	9	-0.008	0.007
2	10	0.036	0.023
2	11	-0.086	-0.095
2	12	0.145	0.016
2	13	0.026	-0.014
2	14	-0.137	0.006
2	15	-0.011	0.032
2	16	0.009	-0.004
2	17	0.224	-0.023
2	18	-0.003	0.010
2	19	0.168	-0.020
2	20	-0.374	0.178
2	21	-0.966	-0.017
2	22	-0.321	-0.060
2	23	0.179	0.003
2	24	0.091	-0.003
2	25	0.016	-0.026
2	26	0.001	-0.000
2	27	0.002	0.000
2	28	-0.056	-0.104
2	29	-0.007	-0.008
2	30	-0.077	0.097
2	31	0.130	0.021
2	32	0.024	-0.002
2	33	0.027	0.001

2	34	-0.001	0.001
2	35	0.016	-0.002
2	36	-0.010	0.011
2	37	0.020	-0.002
2	38	-0.012	0.011
2	39	-0.022	-0.028

LF term	CASSCF energy [cm^{-1}]	NEVPT2 energy [cm^{-1}]	Dominant electronic configurations based on CASSCF orbitals		Contribution to D [cm^{-1}]	Contribution to E [cm^{-1}]
ground state	0	0	$d_{z2}^1 d_{xz}^1 d_{yz}^2 d_{x2-y2}^1 d_{xy}^2$ (38%) $d_{z2}^2 d_{xz}^1 d_{yz}^1 d_{x2-y2}^1 d_{xy}^2$ (33%)	a b		
1st excited state	955.6	1312.4	$d_{z2}^2 d_{xz}^1 d_{yz}^1 d_{x2-y2}^2 d_{xy}^1$ (48%) $d_{z2}^1 d_{xz}^1 d_{yz}^2 d_{x2-y2}^2 d_{xy}^1$ (35%)	c d	-77.598	0.054

transition	Δm_l	Contribution to D
a → c	-	none
a → d	0	strong negative
b → c	0	strong negative
b → d	-	none

Complex 3 (N3)

Multiplicity	Root	D [cm^{-1}]	E [cm^{-1}]
4	1	-56.454	0.069
4	2	7.001	-5.967
4	3	6.710	3.802
4	4	2.889	0.325
4	5	0.404	-0.388
4	6	0.009	-0.115
4	7	0.020	-0.019
4	8	-0.025	-0.000
4	9	-0.011	-0.004
2	0	-0.636	-0.681
2	1	0.977	0.184
2	2	-0.014	0.018
2	3	0.955	-0.046
2	4	0.060	-0.011
2	5	0.007	-0.030
2	6	4.061	0.008
2	7	-2.001	1.326
2	8	-2.014	-1.504
2	9	0.055	0.046
2	10	-0.155	0.046
2	11	0.079	0.116
2	12	0.249	0.074
2	13	-0.002	0.003
2	14	0.012	0.134
2	15	0.000	0.009
2	16	-0.035	-0.035
2	17	0.163	-0.055
2	18	0.004	-0.003
2	19	0.146	-0.010
2	20	-0.258	0.245
2	21	-0.875	-0.928
2	22	-0.435	0.546
2	23	-0.021	-0.018
2	24	0.096	0.005
2	25	0.195	0.043
2	26	0.001	0.000
2	27	0.003	-0.001
2	28	-0.006	-0.029
2	29	0.011	0.001
2	30	-0.073	0.010
2	31	0.112	0.037
2	32	-0.009	-0.001
2	33	0.010	-0.001

2	34	0.000	0.000
2	35	0.011	0.001
2	36	-0.011	0.005
2	37	0.024	-0.002
2	38	-0.009	0.006
2	39	-0.010	-0.021

LF term	CASSCF energy [cm^{-1}]	NEVPT2 energy [cm^{-1}]	Dominant electronic configurations based on CASSCF orbitals		Contribution to D [cm^{-1}]	Contribution to E [cm^{-1}]
ground state	0	0	$d_{z2}^2 d_{xz}^1 d_{yz}^1 d_{x2-y2}^2 d_{xy}^1$ (41%) $d_{z2}^1 d_{xz}^1 d_{yz}^2 d_{x2-y2}^2 d_{xy}^1$ (13%) $d_{z2}^2 d_{xz}^1 d_{yz}^1 d_{x2-y2}^1 d_{xy}^2$ (13%)	a b c		
1st excited state	1430.2	1821.4	$d_{z2}^2 d_{xz}^1 d_{yz}^1 d_{x2-y2}^1 d_{xy}^2$ (40%) $d_{z2}^2 d_{xz}^1 d_{yz}^1 d_{x2-y2}^2 d_{xy}^1$ (22%) $d_{z2}^1 d_{xz}^1 d_{yz}^2 d_{x2-y2}^1 d_{xy}^2$ (20%)	d e f	-56.454	0.069

transition	Δm_l	Contribution to D
a → d	0	strong negative
a → e	-	none
a → f	-	none
b → d	-	none
b → e	1	positive
b → f	0	strong negative
c → d	-	none
c → e	0	strong negative
c → f	1	positive

Complex 4 (NCO)

Multiplicity	Root	D [cm^{-1}]	E [cm^{-1}]
4	1	-49.848	0.164
4	2	7.373	-6.230
4	3	6.539	4.964
4	4	2.115	-0.088
4	5	0.634	-0.651
4	6	-0.007	-0.075
4	7	0.015	-0.015
4	8	-0.015	-0.000
4	9	-0.010	-0.004
2	0	-0.360	-0.884
2	1	0.697	0.256
2	2	-0.022	0.027
2	3	0.554	-0.029
2	4	0.163	-0.016
2	5	-0.032	-0.037
2	6	4.210	-0.001
2	7	-2.025	1.599
2	8	-1.914	-1.584
2	9	-0.039	0.129
2	10	-0.081	0.271
2	11	0.065	0.026
2	12	0.292	0.041
2	13	0.031	-0.001
2	14	0.013	0.108
2	15	-0.030	0.006
2	16	-0.052	-0.035
2	17	0.118	-0.040
2	18	0.006	0.003
2	19	0.118	-0.030
2	20	-0.215	0.186
2	21	-0.789	-0.854
2	22	-0.466	0.432
2	23	-0.027	-0.004
2	24	0.083	0.007
2	25	0.216	0.050
2	26	0.001	0.001
2	27	0.005	-0.001
2	28	0.018	0.032
2	29	0.023	0.002
2	30	-0.095	-0.049
2	31	0.116	0.037
2	32	-0.008	-0.006
2	33	0.002	0.003

2	34	-0.000	0.000
2	35	0.006	0.002
2	36	-0.012	-0.003
2	37	0.020	0.003
2	38	-0.008	0.003

LF term	CASSCF energy [cm^{-1}]	NEVPT2 energy [cm^{-1}]	Dominant electronic configurations based on CASSCF orbitals		Contribution to D [cm^{-1}]	Contribution to E [cm^{-1}]
ground state	0	0	$d_{z2}^2 d_{xz}^1 d_{yz}^1 d_{x2-y2}^2 d_{xy}^1$ (56%) $d_{z2}^1 d_{xz}^2 d_{yz}^1 d_{x2-y2}^2 d_{xy}^1$ (20%) $d_{z2}^1 d_{xz}^1 d_{yz}^2 d_{x2-y2}^2 d_{xy}^1$ (11%)	a b c		
1st excited state	1604.5	2070.8	$d_{z2}^2 d_{xz}^1 d_{yz}^1 d_{x2-y2}^1 d_{xy}^2$ (59%) $d_{z2}^1 d_{xz}^1 d_{yz}^2 d_{x2-y2}^1 d_{xy}^2$ (16%) $d_{z2}^1 d_{xz}^2 d_{yz}^1 d_{x2-y2}^1 d_{xy}^2$ (15%)	d e f	-49.848	0.164

transition	Δm_l	Contribution to D
a → d	0	strong negative
a → e	-	none
a → f	-	none
b → d	-	none
b → e	-	none
b → f	0	strong negative
c → d	-	none
c → e	0	strong negative
c → f	-	none

Complex 5 (NCS)

Multiplicity	Root	D [cm^{-1}]	E [cm^{-1}]
4	1	-50.649	0.153
4	2	6.161	-2.215
4	3	6.355	0.340
4	4	2.276	0.564
4	5	0.194	-0.320
4	6	-0.001	-0.073
4	7	0.017	-0.009
4	8	-0.015	0.000
4	9	-0.010	-0.002
2	0	-0.672	-0.876
2	1	0.580	0.222
2	2	0.125	0.028
2	3	0.599	-0.040
2	4	0.060	-0.003
2	5	0.147	-0.041
2	6	4.018	0.007
2	7	-2.053	0.121
2	8	-1.891	-0.207
2	9	-0.006	-0.063
2	10	-0.050	-0.061
2	11	0.085	0.072
2	12	0.200	0.065
2	13	-0.004	0.037
2	14	-0.048	0.141
2	15	0.010	-0.020
2	16	-0.077	-0.077
2	17	0.125	-0.041
2	18	0.035	-0.000
2	19	0.079	-0.017
2	20	-0.155	0.084
2	21	-0.732	-0.816
2	22	-0.559	0.637
2	23	-0.000	-0.010
2	24	0.073	-0.000
2	25	0.187	0.033
2	26	-0.002	0.002
2	27	0.005	-0.000
2	28	0.012	-0.043
2	29	0.027	-0.000
2	30	-0.022	0.015
2	31	0.058	0.053
2	32	-0.005	0.003
2	33	0.013	-0.009

2	34	0.000	0.000
2	35	0.007	0.002
2	36	-0.012	0.005
2	37	0.015	-0.002
2	38	-0.007	0.006
2	39	-0.008	-0.026

LF term	CASSCF energy [cm^{-1}]	NEVPT2 energy [cm^{-1}]	Dominant electronic configurations based on CASSCF orbitals		Contribution to D [cm^{-1}]	Contribution to E [cm^{-1}]
ground state	0	0	$d_{z2}^2 d_{xz}^1 d_{yz}^1 d_{x2-y2}^2 d_{xy}^1$ (36%) $d_{z2}^2 d_{xz}^1 d_{yz}^1 d_{x2-y2}^1 d_{xy}^2$ (19%) $d_{z2}^1 d_{xz}^1 d_{yz}^2 d_{x2-y2}^2 d_{xy}^1$ (15%)	a b c		
1st excited state	1612.9	2077.2	$d_{z2}^2 d_{xz}^1 d_{yz}^1 d_{x2-y2}^2 d_{xy}^1$ (28%) $d_{z2}^2 d_{xz}^1 d_{yz}^1 d_{x2-y2}^1 d_{xy}^2$ (28%) $d_{z2}^1 d_{xz}^1 d_{yz}^2 d_{x2-y2}^1 d_{xy}^2$ (22%)	d e f	-50.649	0.153

transition	Δm_l	Contribution to D
a → d	-	none
a → e	0	strong negative
a → f	-	none
b → d	0	strong negative
b → e	-	none
b → f	1	positive
c → d	1	positive
c → e	-	none
c → f	0	strong negative

Complex 6 (NCSe)

Multiplicity	Root	D [cm^{-1}]	E [cm^{-1}]
4	1	-48.600	0.112
4	2	5.716	0.591
4	3	6.601	-3.167
4	4	2.224	1.063
4	5	-0.042	-0.166
4	6	-0.008	-0.035
4	7	0.016	-0.001
4	8	-0.014	0.000
4	9	-0.011	-0.001
2	0	-0.806	-0.779
2	1	0.452	0.164
2	2	0.299	0.038
2	3	0.460	-0.034
2	4	0.021	0.004
2	5	0.252	-0.026
2	6	4.020	0.007
2	7	-2.173	-1.003
2	8	-1.883	0.849
2	9	-0.073	-0.221
2	10	0.068	-0.111
2	11	0.080	-0.001
2	12	0.167	0.060
2	13	-0.052	0.065
2	14	-0.051	0.136
2	15	0.036	-0.008
2	16	-0.089	-0.119
2	17	0.122	-0.023
2	18	0.045	-0.001
2	19	0.053	-0.012
2	20	-0.133	0.033
2	21	-0.694	-0.726
2	22	-0.557	0.634
2	23	0.006	-0.004
2	24	0.051	-0.000
2	25	0.203	0.026
2	26	-0.002	0.002
2	27	0.004	0.000
2	28	0.000	-0.071
2	29	0.026	-0.002
2	30	0.010	0.041
2	31	0.033	0.060
2	32	-0.001	0.005
2	33	0.019	-0.013

2	34	-0.000	0.000
2	35	0.007	0.001
2	36	-0.011	0.008
2	37	0.014	-0.004
2	38	-0.006	0.007
2	39	-0.013	-0.031

LF term	CASSCF energy [cm^{-1}]	NEVPT2 energy [cm^{-1}]	Dominant electronic configurations based on CASSCF orbitals		Contribution to D [cm^{-1}]	Contribution to E [cm^{-1}]
ground state	0	0	$d_{z2}^2 d_{xz}^1 d_{yz}^1 d_{x2-y2}^1 d_{xy}^2$ (38%) $d_{z2}^1 d_{xz}^1 d_{yz}^2 d_{x2-y2}^1 d_{xy}^2$ (26%) $d_{z2}^2 d_{xz}^1 d_{yz}^1 d_{x2-y2}^2 d_{xy}^1$ (15%)	a b c		
1st excited state	1695.8	2196.1	$d_{z2}^2 d_{xz}^1 d_{yz}^1 d_{x2-y2}^2 d_{xy}^1$ (44%) $d_{z2}^1 d_{xz}^1 d_{yz}^2 d_{x2-y2}^2 d_{xy}^1$ (26%) $d_{z2}^1 d_{xz}^1 d_{yz}^2 d_{x2-y2}^1 d_{xy}^2$ (10%)	d e f	-48.600	0.112

transition	Δm_l	Contribution to D
a → d	0	strong negative
a → e	-	none
a → f	1	positive
b → d	-	none
b → e	0	strong negative
b → f	-	none
c → d	-	none
c → e	1	positive
c → f	-	none